Properties of Electromagnetic Beams Generated by Ultra-Wide Bandwidth Pulse-Driven Arrays

Richard W. Ziolkowski, *Senior Member, IEEE*

Abstract—**The characteristics of the beams generated by ultra-wide bandwidth electromagnetic systems are central to their practical applications. These characteristics include the rate of beam divergence, the beam intensity, and the energy efficiency. Analytical bounds on the characteristics of beams generated by an arbitrary pulse-driven array are derived and supported with numerical calculations. These bounds extend the meaning of near-field distances or diffraction lengths to the situation where the array driving functions can be broad-bandwidth signals. Particular attention is given to transmitting and receiving array systems which consist of elements that are not large in comparison to the shortest wavelength of significance contained in the signals driving them. The output signals of such systems are time derivatives of the input driving functions. They constitute higher-order beams whose coherence properties are degraded more slowly by diffraction than lower-order beams. The bounds define the extent of these enhancements. It is further shown that for certain measures of performance involving these beam characteristics, a localized wave pulse-driven array can outperform similar continuous-wave-driven arrays. A new type of array is required to realize these localized wave effects—one that has independently addressable elements. The enhanced localization effects are intimately coupled to the proper spatial distribution of broad-bandwidth signals driving the array; i.e., by controlling not only the amplitudes, but also the frequency spectra of the pulses driving the array.**

I. Introduction

LARGE classes of nonseparable space-time solutions to the equations governing many wave phenomena (e.g., scalar wave [1]–[6], Maxwell's [3], [7], Klein–Gordon [8] equations) have been reported recently. When compared with traditional monochromatic, continuous wave (CW) solutions such as Gaussian or piston beams, these localized wave (LW) solutions are characterized by extended regions of localization; i.e., their shapes and/or amplitudes are maintained over much larger distances than their CW analog. These discoveries have prompted several extensive investigations into the possibility of using these LW solutions to drive finite-sized arrays and thus to launch fields having extended localization properties.

Manuscript received March 26, 1991; revised February 19, 1992.

The author is with the Electromagnetics Laboratory, University of Arizona, Tucson, AZ 85721.

IEEE Log Number 9201668.

The physics behind the LW effect involves array elements driven with broad-bandwidth signals whose time dependence varies from location to location. This scheme exploits an additional degree of freedom not used with current CW systems: a designed union between the space and frequency portions of phase space. An LW solution naturally provides this connection; the spatially distributed component waveforms and, therefore, their broad bandwidth spectra are correlated to each other, a self-similarity property inherent in an LW solution. The degree of these correlations can be optimized for a given system. Away from the array the dependence of the current spectrum on location follows from different spectral contributions to the pulse arriving from different locations. A moving interference pattern forms at enhanced distances as the individual waveforms continue to propagate away from their sources. An alternative type of array is necessary to achieve this effect—each array element must be independently addressable so that the appropriate broad bandwidth time signal can be radiated from it. This is in contrast to conventional arrays which deliver the same CW or narrow-bandwidth time signal to each subsystem and then only have independent phase control over each radiating element for beam steering purposes and amplitude control (shading) for the setting of sidelobe levels. Enhanced localization effects can be achieved by driving an array with a properly designed spatial distribution of broad bandwidth signals; i.e., by controlling not only the amplitudes, but also the frequency spectra of the pulses driving the array. Evidence confirming this LW effect with ultrasonic waves in water has been reported [9], [10].

Figures of merit between novel, ultra-wide bandwidth (UWB) pulse solutions and continuous-wave waveforms are difficult to establish. There is no apparent special frequency that can be chosen in a traditional manner to define, for instance, a near-field (Rayleigh) distance or diffraction length when several different broad-bandwidth spectra are involved. Meaningful comparisons of the performance of beams, e.g., the beam divergence, beam intensity and measured beam energy, generated by arrays driven with broad-bandwidth and narrow-bandwidth signals share this difficulty. The traditional performance criteria are based upon CW or, at most, narrow-bandwidth concepts. Moreover, those beam quantities are con-

0018-926X/92$03.00

nected with different portions of the frequency spectra in the broad-bandwidth case, a possibility that does not arise in the CW problem. These issues are particularly acute when the LW solutions are considered. Nevertheless, performance comparisons are desirable and inevitable.

Performance bounds on the quantities associated with a beam generated by an arbitrary pulse-driven array, e.g., beam divergence, transmitted beam intensity and measured beam energy, have been derived analytically for the acoustic case [11]. In particular, the concept of a Rayleigh distance or diffraction length has been extended from the narrow-bandwidth case to a broad-bandwidth configuration. This generalization required the introduction of a frequency value that is characteristic of the frequencies associated with each beam quantity under investigation. It has been shown that there exist useful choices for these characteristic frequency values. The existence of these characteristic frequencies is very important, since it permits a well-defined comparison between the efficiencies and the spreading of the beams generated by CW and UWB pulse-driven arrays. Particular attention has been given to transmitting and receiving array systems consisting of elements that are not large in comparison to the shortest wavelength of significance contained in the signals driving them. The output signals of such systems are related to the input driving functions by several time derivatives. It has been demonstrated that the properties of the resulting beams depend on the higher order moments of the spectra of the input driving functions and that diffraction degrades the coherence of these higher order moments more slowly than its lower orders. A properly designed set of input driving signals having a high degree of correlation in the higher order moments of their spectra will produce a beam that has extended diffraction lengths and localization properties. The localized wave solutions provide an immediate access to this situation. Numerical results supporting these arguments have been given; the experimental results have been reevaluated in terms of these bounds. The reported conclusions [10] that an LW pulse-driven array can outperform its CW counterpart have been reaffirmed by this investigation.

In this paper, the acoustic array performance bounds are extended to the electromagnetic case. This discussion requires an analysis of the transmitting *and* receiving systems since even when only two elements are involved in the UWB case, the measured signal is not simply a replica of the input signal. The issues of beam divergence, transmitted beam intensity and measured beam energy will be addressed in Section II for an arbitrary electromagnetic system consisting of pulse-driven transmitting and receiving arrays. This includes the introduction of the frequencies that are useful characterizations of a set of UWB signals. Several other practical choices for these characteristic frequency values will also be considered. To illustrate the concepts, particular attention will be given in Section III to transmitting and receiving array systems consisting of center-fed, pulse-driven, linear dipole elements that are not large in comparison to the shortest wavelength of significance contained in the signals driving them. In Section IV the transmitting array will be driven with an LW solution, and it will be determined whether or not the resulting beams exhibit the desired enhanced localization effects. Numerical examples will be given to characterize and support this discussion. It will be demonstrated explicitly that a set of ultra-wide bandwidth LW signals can be designed for a pulse-driven array so that it will generate a beam that will outperform its CW counterpart in a variety of applications. In Section V we briefly review and summarize the physics and engineering issues presented here.

The electrically short dipole transmitter–receiver system is chosen to illustrate the results because it is one of the simplest examples of a system whose output signals are related to the input driving functions by several time derivatives. Since the diffraction process affects the higher order moments of the spectra more slowly than lower orders, it will be shown that extended diffraction lengths are associated with these higher derivative systems. Moreover, if the driving signals have a high degree of correlation, it will be shown that these systems also exhibit enhanced transverse localization properties. Thus, a set of UWB signals and an electromagnetic transmitter–receiver system can be designed to realize enhancements of a particular beam parameter. Again, the LW solutions simply provide an immediate access to this situation.

In a series of papers [12]–[18] McIntosh, Pozar, Schaubert, and their coworkers have developed methods which yield the transient waveforms that achieve specific performance criteria for bandlimited transmitter–receiver systems. For instance, the bandlimited current waveforms that produce the maximum signal intensity in a specified direction or the maximum energy in a specified time interval, when they are applied to an array of linear dipole antennas, have been obtained with these methods. The results of their studies have provided bounds on specific performance criteria associated with these bandlimited transmitter–receiver systems. The bounds we present in this paper recover those results and extend them to time-limited signals. Consequently, the present analysis can be readily applied, for example, to the photoconductive switch transmission and reception systems currently under consideration [19]–[25] for applications to radar, microwave spectroscopy, and packaging interconnects. A time-domain interpretation is emphasized here rather than the stepped-frequency approach used in [12]–[18]. The following discussion also highlights multiple time derivative transmitter–receiver systems. It is a known [26]–[33], but not well-appreciated fact that transmission and reception systems have individual responses (e.g., frequency dependent impedances) that must be taken into account when the overall behavior of a UWB pulsed system is analyzed. This issue was addressed briefly in [18] where signals were constructed to optimize the target response for a (one-time derivative) linear dipole antenna transmitter-target-receiver system. Rather than optimizing the performance

of a specific quantity associated with a specific system, a variety of performance criteria are derived here for generic classes of these multiple time derivative transmitter–receiver systems. They are not restricted to the far-field zone of the transmitter or receiver, but are valid even in their Fresnel regions. Moreover, the bounds establish at what distances the corresponding near-to-far-field boundaries occur. They thus provide a useful set of rules of thumb for the evaluation of general UWB systems. The following results could be easily extended to include scattering phenomena in a fashion analogous to [18].

II. Pulsed Beam Performance Bounds

Analytical bounds on the properties of a beam generated by an arbitrary, pulse-driven array are now derived. In our model system the transmitting array consists of N radiating elements, the nth element being driven with the signal f_n over an effective area A_n. The only constraint on the driving functions is that they be continuous. The associated frequency spectra will be labeled $F_n(\omega)$. The total area associated with the array is

$$A = \sum_{n=1}^{N} A_n. \tag{1}$$

The receiving array will be a single receiving element with an effective area A_R. The arguments are readily extended to a multi-element receiving array. This transmitter–receiver system is depicted in Fig. 1.

In general the time domain radiated or received signals in any transmitter–receiver system are not faithful replicas of the input waveforms [23]–[33]. Each component of the transmitting (source, electronics, transmission line, antenna) and receiving (antenna, transmission line, electronics) systems has its own characteristic frequency response. Consequently, the frequency responses of the components of the transmitting and receiving systems, hence the corresponding time domain effects, must be taken into account to model the response of the overall system. This issue is general; each of the system components has the potential to modify any signal it encounters. For instance, the output signal of a transmitter system whose antenna is not large in comparison to the shortest wavelength of significance contained in the time signal driving it, is a time derivative of that input driving function. This time derivative can be understood physically on the basis of energy conversion; it results from the conversion of the electrical energy fed to the antenna into field energy near it. It can also be interpreted as resulting from an effect of the assumption of electrical smallness, i.e., the driving signal will be reflected from the edges of the antenna before the entire pulse shape is radiated from it. This behavior is also represented by a linear dependence in frequency of the transmitter system impedance. By reciprocity, the output of a matched receiver system will also be a time derivative of the signal input into it. The conversion of the field energy into electrical energy imposes a time derivative on the signal. The radiation process itself also introduces a time derivative onto the transmitted signal, i.e., as the signal propagates into the far field of the radiating element, it evolves into a waveform that is the time derivative of the signal created near that element. The time derivative that is associated with the radiation process is expected from the fact that the vector potential $\vec{A}$ is proportional to an integral of the current density at the source points: $\vec{A}(\vec{r}, t) = \mu_0 \int_V J(\vec{r}', t - |\vec{r} - \vec{r}'|/c) d^3\vec{r}'/(4\pi|\vec{r} - \vec{r}'|)$ and the electric field is proportional to the time derivative of the vector potential: $\vec{E} \propto -\partial_t \vec{A}$. This behavior reflects the fact that an antenna does not radiate any dc components. Accounting for all of these effects, one finds that the output signal of this pair of electrically small transmitting and receiving elements is related to the input driving functions by three time derivatives. On the other hand, if the frequency response of either the transmitter or the receiver is constant over the band of interest, that component has no effect on the signal. This would occur if the antenna is not electrically small. Other behaviors, even integrations, are, of course, possible. The model systems to be considered here will be characterized simply by a one-, two-, or three-time derivative output response. They are represented in block-diagram form in Fig. 2.

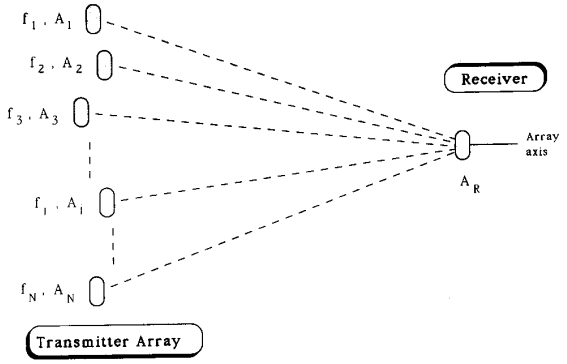

Fig. 1. The signal at the receiver is a linear superposition of the fields generated by driving each transmitting element in the array with a specified time signal.

To aid in the discussion, several concepts must be introduced. The set of driving functions $\{f_j\}_{j=1,N}$ will be said to constitute the *input field*. This situation is analogous to driving the array with a space-time beam, hence the name. The radiating elements take this input field and create the *radiated field*. This is the "field" present when the electrical energy is converted to the field energy to be launched into the medium (free space) by the transmitting dipole array. The *measured field* is the field which has been propagated from the array and measured at the "output" of the receiving antenna. Note that these propagation and measurement processes occur at the end of the propagation phase and in no way influence the behavior of the transmitting antennas or the input field or the radiated field.

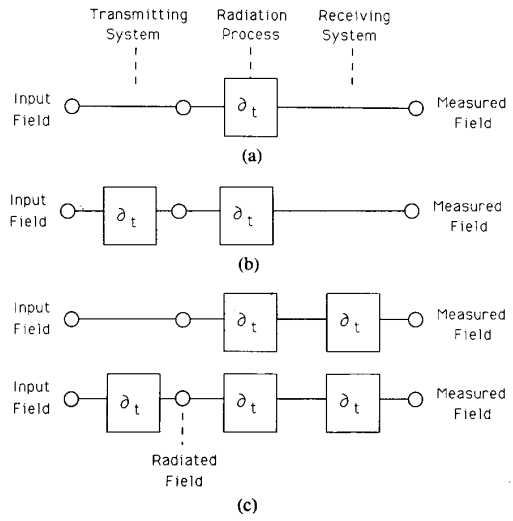

Fig. 2. The output signal of the transmission/reception system model is proportional to multiple time derivatives of the input signals. (a) One-time derivative case. (b) Two-time derivative case. (c) Three-time derivative case.

A. Beam Energy

The input field energy is the energy distributed over the array, the nth element receiving $\mathscr{E}_n^{\text{in}}$ joules:

$$\mathscr{E}_n^{\text{in}} = C_{\text{in}}^2 \int_{-\infty}^{\infty} |f_n(t)|^2 \, dt. \tag{2}$$

The factor C_{in} is a real constant with dimensions consistent with the input field and transmitter system that makes $\mathscr{E}_{\text{in}}$ an energy quantity. If f_n is a voltage, then this factor would have units of inverse impedance. The exact value of C_{in} is model dependent, being defined explicitly by the transmitter associated with the nth radiating element. The total, array-weighted input energy is then taken to be:

$$\mathscr{E}_{\text{in}} \overset{\text{def}}{=} \frac{1}{A} \sum_{n=1}^{N} A_n \mathscr{E}_n^{\text{in}}. \tag{3}$$

This form of the input energy is chosen to account for the amount of the array "real estate" dedicated to each of the driving functions.

An individual (extended) radiating element looks like a point source when the energy it radiates reaches its far field. The time signal measured in the far field at the point $\vec{r}$, which resulted from the radiating element at $\vec{r}_n$ is thus characterized by an amplitude decay factor, $1/R_n$, where $R_n = |\vec{r} - \vec{r}_n|$ is the distance from the center of the nth element to the observation point, and by j-time derivatives ($j = 1$, 2, or 3) of its driving function f_n evaluated at the retarded time $t' = t - R_n/c$. The specific number of time derivatives depends upon the assumed transmitter–receiver configuration of Fig. 2. It is readily shown by a number of methods that the measured far-field amplitude can be represented in the form

$$g(\vec{r}, t) \approx C_j \sum_{n=1}^{N} \frac{A_n}{2\pi c R_n} \partial_t^j f_n(\vec{r}_n, t - R_n/c) \tag{4}$$

which means the measured far-field beam energy is

$$\mathscr{E}_j^{\text{meas}}(\vec{r}) \approx C_j^2 \sum_{m=1}^{N} \sum_{n=1}^{N} \frac{A_m}{2\pi c R_m} \frac{A_n}{2\pi c R_n} \int_{-\infty}^{\infty} dt \cdot \partial_t^j f_m(\vec{r}_m, t - R_m/c) \partial_t^j f_n(\vec{r}_n, t - R_n/c). \tag{5}$$

The real constant C_j has dimensions consistent with the input field and the transmitter–receiver system to make $\mathscr{E}_{\text{in}}$ an energy quantity. Like C_{in}, the exact value of C_j is model dependent. Since bounds are being derived, the constraints on the system are for a maximum response so that it is assumed in (5) that there are no losses or mismatches in the system.

Introducing the terms

$$\mathscr{U}_n^j = A_n \int_{-\infty}^{\infty} dt |\partial_t^j f_n(\vec{r}_n, t)|^2 \tag{6}$$

and the associated correlations measured by the quantity $\Lambda_{j,mn}^{\text{meas}}$

$$\overset{\text{def}}{=} \frac{\int_{-\infty}^{\infty} dt \, \partial_t^j f_m(\vec{r}_m, t - R_m/c) \, \partial_t^j f_n(\vec{r}_n, t - R_n/c)}{\left[\int_{-\infty}^{\infty} dt |\partial_t^j f_m(\vec{r}_m, t)|^2\right]^{1/2} \left[\int_{-\infty}^{\infty} dt |\partial_t^j f_n(\vec{r}_n, t)|^2\right]^{1/2}} \tag{7}$$

one can rewrite the measured energy expression (5) as

$$\mathscr{E}_j^{\text{meas}}(\vec{r}) = C_j^2 \left(\frac{1}{2\pi c}\right)^2 \sum_{m=1}^{N} \sum_{n=1}^{N} \cdot \frac{A_m^{1/2} A_n^{1/2}}{R_m R_n} \Lambda_{j,mn}^{\text{meas}} (\mathscr{U}_m^j)^{1/2} (\mathscr{U}_n^j)^{1/2}. \tag{8}$$

Without any loss of generality, it is assumed the array is a plane perpendicular to the z-axis, e.g., the plane $z = 0$, and that the observation point is along the z-axis, i.e., $\vec{r} = (0, 0, z)$. This simplifies the notations in the following arguments. In particular, one then has for any radiating element that $R_n \geq z$. Applying the Schwartz inequality [34], one finds a bound on the correlation functions:

$$\Lambda_{j,mn}^{\text{meas}} \leq 1 \tag{9}$$

and, hence, a bound on the measured energy:

$$\begin{aligned} \mathscr{E}_j^{\text{meas}}(\vec{r}) &\leq \left(\frac{C_j}{2\pi c}\right)^2 \left[\sum_{n=1}^{N} \frac{(\mathscr{U}^j)_n^{1/2} A_n^{1/2}}{R_n}\right]^2 \\ &\leq \left(\frac{C_j}{2\pi c}\right)^2 \left[\sum_{n=1}^{N} \frac{\mathscr{U}_n^j}{R_n^2}\right] \left[\sum_{n=1}^{N} A_n\right] \\ &= A \left(\frac{C_j}{2\pi c}\right)^2 \left[\sum_{n=1}^{N} \frac{\mathscr{U}_n^j}{R_n^2}\right] \leq C_j^2 \left(\frac{A}{2\pi c z}\right)^2 \left(\frac{\mathscr{U}_j^{\text{meas}}}{A}\right), \end{aligned} \tag{10}$$

where the quantity $\mathscr{U}_j^{\text{meas}} = \sum_{n=1}^{N} \mathscr{U}_n^j$.

We are interested in the energy efficiency of the transmitter-receiver system, a quantity usually quoted as its performance rating. This efficiency is the ratio of the measured energy $\mathscr{E}_j^{\text{meas}}(\vec{r})$ to the input field energy $\mathscr{E}_{\text{in}}$ at the observation point:

$$\Gamma_{j,\text{enrg}}^{\text{meas}}(\vec{r}) \stackrel{\text{def}}{=} \frac{\mathscr{E}_{\text{meas}}(\vec{r})}{\mathscr{E}_{\text{in}}}. \tag{11}$$

The ratio $\Gamma_{j,\text{enrg}}^{\text{meas}}$ can be related to an effective frequency of the radiated field ω_{rad} and the effective frequency of the measured field far from the array ω_{meas} as follows.

With (3) and (10) the desired ratio (11) becomes

$$\Gamma_{j,\text{enrg}}^{\text{meas}} \le \frac{C_j^2}{C_{\text{in}}^2}\left(\frac{A}{2\pi cz}\right)^2 \frac{\mathscr{U}_j^{\text{meas}}}{\mathscr{U}_{\text{in}}}. \tag{12}$$

Recall that we are assuming that the array is driven with a set of UWB signals. To provide a quantitative measure of the frequencies involved in these signals, we introduce the "effective frequency" of the radiated field:

$$\omega_{\text{rad}}^2 \stackrel{\text{def}}{=} \frac{\sum_{n=1}^N A_n \int_{-\infty}^{\infty} dt |\partial_t f_n(\vec{r}_n, t)|^2}{\sum_{n=1}^N A_n \int_{-\infty}^{\infty} dt |f_n(\vec{r}_n, t)|^2} = \frac{\sum_{n=1}^N A_n \int_{-\infty}^{\infty} d\omega\, \omega^2 |F_n(\vec{r}_n, \omega)|^2}{\sum_{n=1}^N A_n \int_{-\infty}^{\infty} d\omega |F_n(\vec{r}_n, \omega)|^2} \tag{13}$$

and the "effective frequency" ω_{meas} of the measured field which for $j = 1$ is set equal to ω_{rad} and for $j \neq 1$ is defined to be

$$\omega_{\text{meas}}^{2(j-1)} \stackrel{\text{def}}{=} \frac{\sum_{n=1}^N A_n \int_{-\infty}^{\infty} dt |\partial_t^j f_n(\vec{r}_n, t)|^2}{\sum_{n=1}^N A_n \int_{-\infty}^{\infty} dt |\partial_t f_n(\vec{r}_n, t)|^2} = \frac{\sum_{n=1}^N A_n \int_{-\infty}^{\infty} d\omega\, \omega^{2j} |F_n(\vec{r}_n, \omega)|^2}{\sum_{n=1}^N A_n \int_{-\infty}^{\infty} d\omega\, \omega^2 |F_n(\vec{r}_n, \omega)|^2} \tag{14}$$

so that

$$\frac{\mathscr{U}_j^{\text{meas}}}{\mathscr{U}_{\text{in}}} = \omega_{\text{rad}}^2 \omega_{\text{meas}}^{2(j-1)}. \tag{15}$$

Recall that the term F_n is the Fourier transform of the driving signal f_n. The effective frequency ω_{rad} is a measure of the spectral energies launched into the medium in our model. It is a ratio of the array-weighted accumulation of the contributions to the energy spectrum of the field near the array face and the array-weighted accumulation of the energy spectra of the signals driven into the array. On the other hand, the measured frequency ω_{meas} accounts for the spectral energies measured in the receiver of our model. It replaces the energy spectrum of the field near the array face with the energy spectrum of the measured field far from the array. Note that the effective frequencies are quantities that characterize *by a single frequency value* all of the UWB components contained in all of the signals involved in the radiation and measurement processes.

The bound (12) on the energy efficiency (11) now becomes

$$\Gamma_{j,\text{enrg}}^{\text{meas}} \le \frac{C_j^2}{C_{\text{in}}^2}\left(\frac{A\omega_{\text{rad}}}{2\pi cz}\right)^2 \omega_{\text{meas}}^{2(j-1)} = \frac{C_j^2}{C_{\text{in}}^2}\left(\frac{A}{\lambda_{\text{rad}} z}\right)^2 \omega_{\text{meas}}^{2(j-1)} \tag{16}$$

where $\lambda_{\text{rad}} = 2\pi c/\omega_{\text{rad}}$. Introducing the Rayleigh distance based upon the effective frequency of the radiated field:

$$L_{\text{rad}} \stackrel{\text{def}}{=} \frac{A\omega_{\text{rad}}}{2\pi c} = \frac{A}{\lambda_{\text{rad}}} \tag{17}$$

this means

$$\Gamma_{j,\text{enrg}}^{\text{meas}} \le \frac{C_j^2}{C_{\text{in}}^2}\left(\frac{L_{\text{rad}}}{z}\right)^2 \omega_{\text{meas}}^{2(j-1)}. \tag{18}$$

It is advantageous to renormalize the efficiency $\Gamma_{j,\text{enrg}}^{\text{meas}}$ by the term $(C_j^2/C_{\text{in}}^2)\omega_{\text{rad}}^{2(j-1)}$. This represents a weighting of the time derivatives, which result from the transmitting and receiving arrays, by the physical constants associated with those arrays and by the effective frequency associated with their conversion of the input energy to the radiated field energy or reciprocally, from the radiated to the measured field energy. With this renormalization one obtains

$$\tilde{\Gamma}_{j,\text{enrg}}^{\text{meas}} \stackrel{\text{def}}{=} \frac{\Gamma_{j,\text{enrg}}^{\text{meas}}}{\left(C_j^2/C_{\text{in}}^2\right)\omega_{\text{rad}}^{2(j-1)}} \le \left(\frac{\omega_{\text{meas}}}{\omega_{\text{rad}}}\right)^{2(j-1)}\left[\frac{L_{\text{rad}}}{z}\right]^2. \tag{19}$$

This is the desired bound on the measured energy efficiency of a pulse-driven array. It suggests that for the UWB signal case we introduce the Rayleigh distance

$$L_{j,\text{enrg}}^{\text{meas}} = \left(\frac{\omega_{\text{meas}}}{\omega_{\text{rad}}}\right)^{(j-1)} L_{\text{rad}} \tag{20}$$

which allows us to rewrite (19) as

$$\tilde{\Gamma}_{j,\text{enrg}}^{\text{meas}} \le \left(\frac{L_{j,\text{enrg}}^{\text{meas}}}{z}\right)^2. \tag{21}$$

The diffraction length $L_{j,\text{enrg}}^{\text{meas}}$ given by (20) can be designed for a multiple derivative system to be substantially greater than L_{rad} by a suitable choice of the UWB signals driving the array, e.g., the LW signals. In particular, for a one time derivative system, (20) indicates that $L_{1,\text{enrg}}^{\text{meas}} = L_{\text{rad}}$. In contrast, for a three time derivative system it gives $L_{3,\text{enrg}}^{\text{meas}} = (\omega_{\text{meas}}/\omega_{\text{rad}})^2 L_{\text{rad}}$. Since the higher order moments of an ultra-wide bandwidth spectrum can be designed to occur higher in frequency than the lower order ones, a higher derivative system provides an extended near-field region; and, hence, the energy efficiency of the beam will be maintained in that region and will be enhanced beyond it. This means that diffraction affects the higher order coherence properties of a beam more slowly than its lower orders. This result is depicted graphically in Fig. 3.

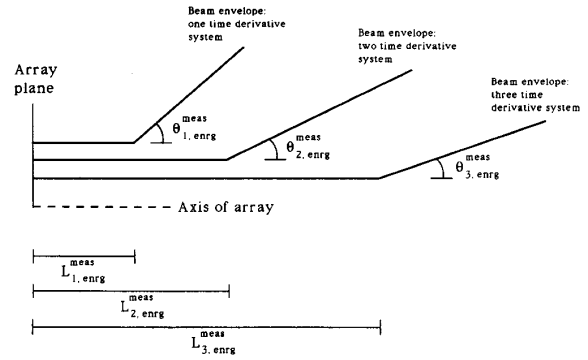

Fig. 3. Diffraction affects the higher order coherence properties of a beam generated by a UWB pulse-driven array more slowly than its lower orders. The envelopes of the measured energy of a beam generated by an optimal one, two, and three time derivative UWB transmitter–receiver system are defined by their diffraction lengths and the rate of spread of the beam in the region beyond their diffraction lengths.

In a CW or narrow-band case each element in the transmitter array of this system is driven with the same CW signal having the angular frequency ω_{CW} so that $\int dt|\partial_t^j f|^2 = \omega_{CW}^{2j}\int dt|f|^2$. Therefore, in the CW case one has

$$\omega^{CW}_{meas} = \omega^{CW}_{rad} \equiv \omega_{CW} \tag{22}$$

and the diffraction lengths associated with the CW measured field are (for all j)

$$L^{CW}_{j,enrg} = L^{CW}_{rad} = \frac{A}{\lambda_{CW}}. \tag{23}$$

If each of the radiating elements have the same area $A_n = A_0$ so that $A = NA_0$, (19) gives

$$\tilde{\Gamma}^{CW}_{j,enrg} \le \left(\frac{L^{CW}_{rad}}{z}\right)^2 = N^2\left(\frac{A_0}{\lambda_{CW}\, z}\right)^2; \tag{24}$$

i.e., the CW energy efficiency is bounded by the coherent superposition of all of the radiating elements. For $j = 1$ this result also recovers the antenna theorem [35].

These results indicate that when a multiple time derivative system is used, the measured energy of the beam generated by a UWB pulse-driven array has a diffraction length that can be made substantially larger than the beam generated by the same array driven with a set of CW or narrow-band signals at the frequency ω_{rad}. For instance, consider a transmitter–receiver system with a three time derivative ($j = 3$) behavior. The renormalized energy efficiency of such a system satisfies the bound:

$$\tilde{\Gamma}^{meas}_{3,enrg} \le \left[\frac{\omega_{meas}}{\omega_{rad}}\right]^4\left(\frac{L_{rad}}{z}\right)^2. \tag{25}$$

The ratio of the measured energy efficiencies of beams generated by such CW and UWB pulse-driven arrays can therefore be written as

$$\frac{\tilde{\Gamma}^{UWB}_{3,enrg}}{\tilde{\Gamma}^{CW}_{3,enrg}} \equiv \frac{\Gamma^{UWB}_{3,enrg}}{\Gamma^{CW}_{3,enrg}} \sim \left(\frac{L^{UWB}_{3,enrg}}{L_{rad}}\right)^2 \equiv \left(\frac{\omega_{rad}}{\omega_{CW}}\right)^2\left[\frac{\omega_{meas}}{\omega_{CW}}\right]^4. \tag{26}$$

Consequently, the condition for a UWB pulse-driven array to be more energy efficient than the CW pulse-driven array is simply

$$\omega^2_{meas}\,\omega_{rad} > \omega^3_{CW}. \tag{27}$$

If, for example, one sets $\omega_{CW} = \omega_{rad}$, the condition for the UWB array to be more efficient than the CW array is simply $\omega_{meas} > \omega_{rad}$. Thus, the energy efficiency of an UWB system increases over the comparable CW system at $\omega_{CW} = \omega_{rad}$ as the square of the diffraction length ratio or, equivalently, as the fourth power of the frequency ratio ($\omega_{meas}/\omega_{CW}$). As has been demonstrated theoretically [11] and experimentally [10], this improvement is readily achieved using a variety of LW solutions as the UWB driving signals. In fact, more than an order of magnitude increase in the measured field energies can be achieved. These issues will be discussed further in Section IV.

The issues to be reemphasized at this point are that 1) one has a choice of the type of transmitter–receiver system, and 2) for that system one can design input driving functions that maximize the differences between the performance of a UWB input field and the corresponding CW one. The LW solutions are just one means to this end. Optimization routines can be developed to further enhance the UWB results [36].

B. Beam Intensity

In many applications it is not the signal energy that is the quantity of interest, but rather the intensity delivered to a point in space-time. This is particularly true in the case of a scattering application such as radar. Many radar systems rely simply on the detection of the peak intensity scattered by the target. Another example deals with a microscopic situation. The force a charged particle experiences is related to the instantaneous field strength it experiences, not the average over time. Furthermore, in many weapons applications, the power delivered by the beam is the important quantity, not its energy. For example, in many high power microwave effects applications it is the maximum intensity of a pulse that causes an upset in the state of a computer chip, whereas the pulse energy can lead to a thermal mode burnout of the device. It will be shown below that the bandwidth of the signal on the "target" is the quantity that determines the maximum intensity there. This property gives a significant advantage to a UWB pulse-driven array over a CW array because of the inherent broad bandwidths of its input signals.

Consider now the measured far-field beam intensity

$$\mathscr{I}_j^{\text{meas}}(\vec{r},t) = \frac{C_j^2}{A_R}\sum_{m=1}^{N}\sum_{n=1}^{N}\frac{A_m}{2\pi cR_m}\frac{A_n}{2\pi cR_n} \cdot \partial_t^j f_m(\vec{r}_m, t - R_m/c)\,\partial_t^j f_n(\vec{r}_n, t - R_n/c) \tag{28}$$

where A_R is an area associated with the receiving antenna. This expression represents the power density (W/m^2) at the receiver located at a given point in space at a given time. Proceeding as in the energy case, one obtains the following bound for the measured intensity normalized by the array weighted input energy:

$$\frac{\mathscr{I}_j^{\text{meas}}(\vec{r},t)}{\mathscr{E}_{\text{in}}} \le \frac{C_j^2}{C_{\text{in}}^2 A_R}\left(\frac{A}{2\pi cz}\right)^2 \cdot \frac{\sum_{n=1}^{N} A_n |\partial_t^j f_n(\vec{r}_n, t - R_n/c)|^2}{\sum_{n=1}^{N} A_n \int_{-\infty}^{\infty} dt |f_n(\vec{r}_n,t)|^2}. \tag{29}$$

Note that this expression represents many time values. To reduce it to a more meaningful quantity, we will consider only the maximum of the intensity time history at a given spatial location $\mathscr{I}_{\text{meas}}^{\max}(\vec{r})$. This operation will be denoted by $\max_t$, i.e., $\mathscr{I}_{\text{meas}}^{\max}(\vec{r}) = \max_t \mathscr{I}_{\text{meas}}(\vec{r},t)$. This allows one to define an intensity pattern and to discuss the associated side-lobe levels even in the broad bandwidth case. Introducing the term

$$\Upsilon_j^{\text{meas}} \overset{\text{def}}{=} \frac{\max_t \sum_{n=1}^{N} A_n |\partial_t^j f_n(\vec{r}_n,t)|^2}{\sum_{n=1}^{N} A_n \int_{-\infty}^{\infty} dt |\partial_t^j f_n(\vec{r}_n,t)|^2} \tag{30}$$

and noticing that the maximum of a time shifted time signal is bounded by the maximum of that signal without the time shift, one can obtain the maximum field intensity normalized by the array weighted input energy from (29) as

$$\frac{(\mathscr{I}_j^{\text{meas}})_{\max}(\vec{r})}{\mathscr{E}_{\text{in}}} \le \frac{C_j^2}{C_{\text{in}}^2 A_R}\left(\frac{A}{\lambda_{\text{rad}} z}\right)^2 \omega_{\text{meas}}^{2(j-1)}\Upsilon_j^{\text{meas}}. \tag{31}$$

The renormalized version of this quantity produces a bound on the efficiency of the measured beam intensity:

$$\tilde{\Gamma}_{j,\text{int}}^{\text{meas}} \overset{\text{def}}{=} \frac{\mathscr{I}_j^{\text{meas}}(\vec{r},t)}{\omega_{\text{rad}}^{2j-1}\left[C_j^2/(C_{\text{in}}^2 A_R)\right]\mathscr{E}_{\text{in}}} \le \left(\frac{\omega_{\text{meas}}}{\omega_{\text{rad}}}\right)^{2(j-1)}\frac{\Upsilon_j^{\text{meas}}}{\omega_{\text{rad}}}\left[\frac{A}{\lambda_{\text{rad}} z}\right]^2 = \left(\frac{L_{j,\text{int}}^{\text{meas}}}{z}\right)^2 \tag{32}$$

where the diffraction length associated with the measured beam intensity is

$$L_{j,\text{int}}^{\text{meas}} \overset{\text{def}}{=} \left(\frac{\omega_{\text{meas}}}{\omega_{\text{rad}}}\right)^{(j-1)}\left[\frac{\Upsilon_j^{\text{meas}}}{\omega_{\text{rad}}}\right]^{1/2} L_{\text{rad}} = \left(\frac{\Upsilon_j^{\text{meas}}}{\omega_{\text{rad}}}\right)^{1/2} L_{j,\text{enrg}}^{\text{meas}}. \tag{33}$$

This diffraction length is generally different from the one associated with the measured beam energy. It can be made $[\Upsilon_j^{\text{meas}}/\omega_{\text{rad}}]^{1/2}$ times larger with a proper design of the input field.

The term Υ_j^{meas} is simply the ratio of the maximum of a function to its time-averaged value. In a CW tone burst case (finite, time-windowed CW signal), the maximum of the jth time derivative of the driving function squared is ω_{CW}^{2j} and the energy of that signal is ω_{CW}^{2j} times half its time record length T_{RL}. Thus the desired ratio in this CW case becomes

$$\Upsilon_{j,\text{meas}}^{\text{CW}} = \frac{2}{T_{\text{RL}}} = \frac{2}{mT_{\text{CW}}} = \frac{\omega_{\text{CW}}}{m\pi} \tag{34}$$

where the last expression assumes there are m CW cycles in the record length time: $T_{\text{RL}} = mT_{\text{CW}}$. Therefore, if one drives the array with a CW signal for a long time (m is large), the value of T_{RL} is large and, hence, that of $\Upsilon_{j,\text{meas}}^{\text{CW}}$ is small. In contrast, for example, the LW driving signals all have broad bandwidths, so that one can achieve a very large instantaneous value of the square of the signals with a small average value over a time period comparable to the CW case. The entire bandwidth controls the behavior of the measured beam intensity rather than, as in the energy efficiency case, a particular frequency value. Note that even for comparable levels of the derivatives of the input signals, narrow-bandwidth signals must necessarily have larger time record lengths than broad-bandwidth signals. Thus one can design the LW driving functions to obtain for any $j = 1$, 2, or 3, the condition: $\Upsilon_{j,\text{meas}}^{\text{LW}} > \Upsilon_{j,\text{meas}}^{\text{CW}}$. Therefore, since

$$\frac{\tilde{\Gamma}_{j,\text{int}}^{\text{UWB}}}{\tilde{\Gamma}_{j,\text{int}}^{\text{CW}}} \sim \left(\frac{\omega_{\text{meas}}^{\text{UWB}}}{\omega_{\text{CW}}}\right)^{2(j-1)}\left(\frac{\omega_{\text{rad}}^{\text{UWB}}}{\omega_{\text{CW}}}\right)^2\left[\frac{\Upsilon_{j,\text{meas}}^{\text{UWB}}}{\Upsilon_{j,\text{meas}}^{\text{CW}}}\right] \tag{35}$$

one can obtain a much larger instantaneous field intensity with a properly designed UWB input field, such as a LW solution, than in the corresponding CW case.

Note that an energy expression represents an average of the signal intensity over time. Because they contain a broad set of frequencies, the peak intensities in a UWB, hence LW, beam can be made quite high as noted above. However, because the drive functions defined, for example, by a LW solution and, hence, the input field are generally unipolar and because they can persist with low amplitude "tails" over several time periods of the corresponding effective frequency CW signal, this characteristic becomes diminished when the time average is applied. Thus low average energies result in the UWB case, in contrast to high peak intensities. Consequently, the performance characteristics of a CW or narrow-bandwidth beam are favored by energy arguments; and those of a UWB, hence LW, beam are favored in intensity comparisons.

C. Beam Width

The rate of divergence of the beam generated by a pulse-driven array can now be obtained as well. The rate

of expansion of a beam can be quantified by measuring the radius at which its energy profile has decreased to half its maximum value in the plane $z = \text{const}$ away from the aperture. This radius value, the half-width at half-maximum (HWHM) of the energy profile, is a good measure of the transverse localization of the beam.

Consider again the measured field energy expression (8). The terms $\Lambda^{\text{meas}}_{j,\text{mn}}(\vec{r})/(R_m R_n)$ clearly control the observation point dependence of the beam. Since the convolutions

$$\int_{-\infty}^{\infty} dt\, \partial_t^j f_m(\vec{r}_m, t - R_m/c)\, \partial_t^j f_n(\vec{r}_n, t - R_n/c)$$

$$= \int_{-\infty}^{\infty} d\tau\, \partial_t^j f_m(\vec{r}_m, \tau)\, \partial_t^j f_n(\vec{r}_n, \tau - [R_n - R_m]/c)$$

$$\equiv \left[A_m A_n \mathscr{U}_m^j \mathscr{U}_n^j\right]^{1/2} \Lambda^{\text{meas}}_{j,\text{mn}}(\vec{r}), \tag{36}$$

the beam energy decreases as the array driving functions become uncorrelated. In the far-field the distance factor $(R_m R_n)^{-1} \sim z^{-2}$ and the time factor $[R_n - R_m]/c \sim (\vec{r}_m - \vec{r}_n)\cdot\vec{r}/cz$. Thus the off-axis behavior rests solely with the convolution terms $\Lambda^{\text{meas}}_{j,\text{mn}}(\vec{r})$ in (36). Those terms decrease to half their value when their arguments experience a time shift approximately equal to a quarter of their characteristic time period. This occurs when: $[R_n - R_m]/c \sim T_{\text{meas}}/4 = (\pi/2\omega_{\text{meas}})$. Accounting for the variations in the driving time signals across a planar array, the HWHM of the far-field measured energy profile occurs at the radius: $\rho^{\text{meas}}_{\text{HWHM,enrg}} \approx (\lambda_{\text{meas}}/4\, d_{\max})z$, where $\lambda_{\text{meas}} = 2\pi c/\omega_{\text{meas}}$ and $d_{\max}$ is the largest distance between the significant, distinct time signals in the array, usually the maximum radius of an element in the array. The rate of divergence of the beam then is simply

$$\theta^{\text{meas}}_{\text{enrg}} = \frac{\rho^{\text{meas}}_{\text{HWHM,enrg}}}{z} \approx \frac{\lambda_{\text{meas}}}{(4\, d_{\max})}. \tag{37}$$

The beam generated by a CW pulse-driven array of diameter $D = 2\, d_{\max}$ will then diverge for $j = 1$, 2, or 3 at the rate:

$$\theta^{\text{meas}}_{\text{enrg,CW}} \approx \frac{\lambda_{\text{CW}}}{2D}. \tag{38}$$

Because one can control *by design* the correlation properties of the constituent time signals as well as satisfaction of the effective frequency condition (27) (i.e., the relative arrival times and the amounts of the various frequency components), the energy profile of the beam generated by a UWB pulse-driven array can be made more localized than the corresponding CW beam:

$$\frac{\theta^{\text{meas}}_{\text{enrg,UWB}}}{\theta^{\text{meas}}_{\text{enrg,CW}}} = \frac{\omega_{\text{CW}}}{\omega^{\text{UWB}}_{\text{meas}}} < 1. \tag{39}$$

The CW "antenna theorem" [35] can now be extended to a general UWB system. With (39), the product of the source area and the far-field beam angular spread (solid angle) is on the order of the measured wavelength squared. In particular, if the effective area of the array $A \approx \pi\, d_{\max}^2$, then

$$A \times \left[\pi(\theta^{\text{meas}}_{\text{enrg}})^2\right] = \frac{\pi A}{(4\, d_{\max})^2}\lambda^2_{\text{meas}}$$

$$\approx \left(\frac{\pi}{4}\right)^2 \lambda^2_{\text{meas}} \sim \lambda^2_{\text{meas}}. \tag{40a}$$

This relation can also be rewritten in the form

$$L^{\text{meas}}_{j,\text{enrg}} \times \left(\frac{\lambda_{\text{meas}}}{\lambda_{\text{rad}}}\right)^{j-2} \times \left[\pi(\theta^{\text{meas}}_{\text{enrg}})^2\right] \approx \lambda_{\text{meas}} \tag{40b}$$

which connects the measured beam energy diffraction length and beam spread with the measured effective wavelength. Thus the beam created by *any* transmitter–receiver system will be constrained to satisfy (40a) and (40b).

It must be remembered that the intensity and the energy profiles of a beam behave differently in the general UWB case. They are controlled by different, but related properties of the spectra of the input field. This difference between the measured intensity and energy beam profiles has been observed experimentally [10], [11]. Thus, one can also introduce a beam width for the intensity as was done with the diffraction length. In general this maximum intensity (in time) beam width $\theta^{\text{meas}}_{\text{int}}$ will be narrower than the energy beam width $\theta^{\text{meas}}_{\text{enrg}}$, i.e.,

$$\theta^{\text{meas}}_{\text{int}} \le \theta^{\text{meas}}_{\text{enrg}}. \tag{41}$$

The equality occurs for any CW case. This is again a result of the intensity being a point quantity rather than an average one as is the energy. As the field expands, the off-axis field values become more spread out in time giving a wider, more uniform energy profile. However, this expansion also causes the maximum intensity in time to decrease more for any spatial point further off-axis in any given plane transverse to the propagation direction since the wavefront must travel further to reach it. Accounting for this difference to determine the spread of the profile of the beam's maximum intensity (in time), one finds approximately that $L^{\text{meas}}_{j,\text{int}} \times (\lambda_{\text{meas}}/\lambda_{\text{rad}})^{j-2} \times [\pi(\theta^{\text{meas}}_{\text{int}})^2] \approx \lambda_{\text{meas}}/2$ so that $\theta^{\text{meas}}_{\text{int}} \sim [4\Upsilon^{\text{meas}}_j/\omega_{\text{rad}}]^{-1/4}\, \theta^{\text{meas}}_{\text{enrg}}$. The resulting narrower intensity profiles of a UWB system may have significant implications for several potential applications.

D. Discussion

The results for the measured beam intensity and energy are clearly dependent on the system model since the latter controls the number of time derivatives involved in the representations of the beam quantities. From an engineering point of view they indicate that one can use broadbandwidth systems to advantage if they are designed properly. It is also now apparent that in any comparisons between a CW case and a UWB, hence LW, case, the choice of the CW frequency is a crucial factor. Note again

that in the CW case, the input, radiated, and measured fields are simply related by powers of the frequency, ω_{CW}, a single constant. There is essentially no difference between the radiated, propagated, and measured fields even if there is a spatial variation in the field. However, in the UWB case, there are large differences; and all of these effects must be taken into account. The arriving time signals are spatially distributed, each bringing to the receiver a different broad-bandwidth spectrum. Because of the different time derivatives involved, different portions of the frequency spectra of those signals will control the associated beam characteristics. The actual transmitter/receiver system configuration then becomes extremely important if enhanced performances are desired, and it must be tailored to the particular beam parameter of interest to realize those enhancements.

The effective frequency value ω_{rad} is an appealing quantity for comparison purposes since it is defined in terms of the variance of the spectra of the input field. When the transmitter imposes a time derivative on the radiated signal, it measures the frequency content near the array (after the array has modified the signals). Moreover, for the systems whose far-field signals involves only one time derivative, it has removed the dc components which are not present there. On the other hand, ω_{rad} does not address an essential difference between the input field and the radiated field. Consider the input set of driving functions. These functions deliver the energy to the array. The electronics driving the array will expend this energy to create these signals, to pass them to the radiating elements, and to radiate them. The driving function spectra have an upper frequency ω_{max} above which they contain very little energy. If the driving functions are time-limited, these tails extend out to an infinite frequency. Moreover, these signals will generally have dc components that carry a great deal of the input energy which will remain in the very near field of the transmitting array. The standard engineering criterion would be the "3 dB" point of the composite energy spectrum delivered to the array (provided that the spectrum is low-pass beyond this point); i.e., one usually choses the value $\omega_{max} = \omega_{3\,dB}$, the frequency at which the total energy spectrum has decreased to half its value. This frequency value is a measure of how much energy is actually used to drive the transmitter system. The frequency value ω_{rad} may be too high for a "fair" CW comparison case since it has eliminated the lower frequency components. As the value of ω_{CW} decreases from ω_{rad}, the relative enhancements of the UWB system increase for any number of time derivatives. For instance, if one were to choose $\omega_{CW} = \omega_{3\,dB}$, then from (26) one finds

$$\frac{\tilde{\Gamma}^{UWB}_{j,enrg}}{\tilde{\Gamma}^{CW}_{j,enrg}} \sim \left(\frac{\omega^{UWB}_{rad}}{\omega_{3\,dB}}\right)^{2j}\left[\frac{\omega^{UWB}_{meas}}{\omega^{UWB}_{rad}}\right]^{2(j-1)} \equiv \left(\frac{\omega^{UWB}_{rad}}{\omega_{3\,dB}}\right)^{2(j-1)}\left[\frac{L^{UWB}_{3,enrg}}{L_{3\,dB}}\right]^{2}, \quad (42)$$

where $L_{3\,dB} = A\,\omega_{3\,dB}/(2\pi c)$. Substantial enhancements over the CW case would then be observed even for a $j = 1$ UWB system. Note that in [9] and [10], the second e-folding point of the LW array-weighted energy spectrum was chosen for the frequency value ω_{max}; it coincided with ω_{rad}. In contrast to the 3 dB value, this choice was much higher in frequency: $\omega_{rad} \sim 3.59\ \omega_{3\,dB}$.

The effective frequency of the radiated field must be altered somewhat when the observation point is in the near field of an individual radiating element. One must then take into account all of the near-field terms (static and induction terms as well as the radiation term). Including these lowest frequency components of the fields near each radiating element in the calculation of the effective frequency of the radiated field, one is led to a value Ω_{rad} rather than ω_{rad}. This value Ω_{rad} would be a better choice for the comparison CW frequency instead of ω_{rad} since it represents all of the energy delivered initially to the beam in the medium. Unfortunately, it is more difficult to calculate in practice. However, because energy is lost to these near-field components as the beam forms and propagates away from the array elements, one knows that $\Omega_{rad} \leq \omega_{rad}$ [11].

What does happen if the transmitting and receiving antennas are designed only to reproduce the fields incident on them? From (19) and (24) the ratio of the CW and UWB beam energy and intensity efficiencies in this case is

$$\frac{\Gamma^{UWB}_{1,enrg}}{\Gamma^{CW}_{1,enrg}} \sim \left(\frac{L^{UWB}_{1,enrg}}{L^{CW}_{1,enrg}}\right)^2 \equiv \left(\frac{\omega_{rad}}{\omega_{CW}}\right)^2 \quad (43)$$

$$\frac{\Gamma^{UWB}_{1,int}}{\Gamma^{CW}_{1,int}} \sim \left(\frac{\omega_{rad}}{\omega_{CW}}\right)^2 \times \left(\frac{\Upsilon^{UWB}_{1,meas}}{\Upsilon^{CW}_{1,meas}}\right). \quad (44)$$

Thus, the energy efficiency for the two types of beams is comparable for a one derivative system with the choice of $\omega_{CW} = \omega_{rad}$. On the other hand, one can achieve a diffraction length for the beam intensity and a beam intensity enhancement which is $(\Upsilon^{UWB}_{1,meas}/\Upsilon^{CW}_{1,meas})$ times larger than those associated with the CW beam. The rise-times of the input field signals control the beam energy diffraction length; the bandwidth of those signals controls the diffraction length of the beam intensity. Note that if the near-field behavior is included and one chooses $\omega_{CW} = \Omega_{rad}$, one then finds that the UWB beams can be more energy efficient than their CW counterpart even for a one time derivative transmitter-receiver system, i.e., $\Gamma^{UWB}_{1,enrg}/\Gamma^{CW}_{1,enrg} = (\omega_{rad}/\Omega_{rad})^2 \geq 1$.

Equation (43) explains immediately one approach that one could take to design a set of driving functions to maximize the beam energy efficiency for this system. One would try to design functions with as fast a rise time as possible, thereby maximizing their first derivatives, hence, the corresponding ω_{rad}. This is, in essence, the basis of the EM missile concept [37]. It is trivial to design a set of driving functions that have finite energy but have a discontinuity in their first derivative. Driving an array with

such an infinite bandwidth signal can result in a beam that remains localized to infinity. In fact, as was shown recently [38], the energy decay of such a beam is $1/r$ rather than $1/r^2$. On the other hand, an infinite bandwidth array is not available because of hardware (electronics, etc.) limitations, so that such a case cannot be realized physically. One then returns immediately to having to make a choice as to what frequency one uses for quantitative comparisons. In a practical application, if there were a frequency cut-off intrinsic to the system that could not be avoided, one would have to determine if this cut-off would affect the effective frequency values or not. Any CW comparisons should then be made with a CW frequency value which fairly represents the frequencies contained in the UWB driving signals.

The difference between the one, two, and three time derivative behaviors of the fields in the far-zone also points out another characteristic of pulse-driven arrays. Because of these time derivative differences, one generally has $\omega_{\text{meas}} > \omega_{\text{rad}}$, which represents a difference between the frequency content of the fields launched from the array into the medium near that array and the spectra reaching the far-field region. This property of the near-field and far-field frequency spectra is associated with the fact that the lower frequency components are radiated less efficiently into the far-field and require more energy to excite them. The beam, in essence, can shed its lower frequencies as it propagates. If the input signals and the radiating elements are not designed properly to account for this *frequency shedding* property, the beam generated by the array will quickly lose its lower frequency components as it propagates, resulting in a degradation of the shape of the beam and an ensuing increase in cost of its energy efficiency.

This frequency shedding property is intrinsically associated with the diffraction process. The measured energy bound for the one-derivative system indicates that the diffraction length is associated with the second moment of the power spectra of the input signals. On the other hand, the measured energy bound for the three-derivative system indicates that the corresponding diffraction length is associated with the sixth moment of the power spectra of the input signals. In either case, the diffraction length is a measure of the coherence of the measured beam energy. The difference in these diffraction lengths implies that the diffraction process affects the coherence of the higher order moments of the spectra more slowly than lower orders, as noted in Section II-A.

Even if there were not a gain in efficiency of the radiated field in the UWB case, the increase in the distance over which localization can be maintained may be more significant. Any performance comparison clearly depends on the intended application of the beam. If one is interested in secure communications, for example, the maintenance of beam quality with low sidelobe levels is of the utmost importance. If one is simply interested in weapons applications, then one would expect that the more efficiency one has, the better. This is not true if the trade-off for large efficiencies is large sidelobe levels. Fratricide issues can become extremely important. In particular, why not attempt to drive the array with a CW frequency corresponding to the absolute bandwidth (i.e., at the highest frequency handled by the system)? The bound (19) would suggest such a choice if the largest beam energy efficiency is desired. One finds that for a given set of radiating elements, going to higher frequency values in the CW case maintains the on-axis efficiency at the cost of very large sidelobes, the so-called grating lobes. These grating lobes appear when the wavelength of the CW signal becomes smaller than the element spacings. They do not appear when the proper broad bandwidth driving functions are used. For communication and remote sensing applications, this cost of maintaining the beam brightness may be too high. As shown in [36] and below, a UWB signal set can be designed to drive an array and produce a beam with high efficiency and very low sidelobe levels. Another possibility would be to drive each element in an array with the same broad-bandwidth signal $f_0(t)$. If the resulting input energy is identical to the UWB case: $A\int_{-\infty}^{\infty}|f_0|^2\,dt = \sum_{n=1}^{N}A_n\int_{-\infty}^{\infty}dt|f_n|^2$, the corresponding frequency spectrum $F_0(\omega)$ satisfies the relation: $\omega^{2j}|F_0(\omega)|^2 = \sum_{n=1}^{N}(A_n/A)\omega^{2j}|F_n(\omega)|^2$ for any integer j. Thus the effective frequency ω_{meas}, hence the diffraction length associated with the measured energy of the beam, would be the same in both cases. Although this approach seems straightforward, it has two drawbacks. The first is the loss in localization that occurs when the spatial degree of freedom is not utilized. To achieve the entire spectrum associated with the set of UWB driving functions, the time $f_0(t)$ must necessarily be longer in time than any of those UWB signals. Thus the convolutions will persist for a longer time giving a larger transverse distance, hence, faster rate of divergence than with the UWB beam. This faster rate of divergence for a beam generated by an array driven with a single broad-bandwidth time signal having the same frequency content as the UWB case has been confirmed experimentally. The second drawback is one of practicality. The requisite signal $f_0(t)$ will be much more complicated than any of the individual UWB driving signals; and hence, more complex waveform generators and radiators would be required to produce it. This increase in complexity combined with the decrease in localization would severely limit the usefulness of such an input field scheme.

The extension of the near field and the narrowing of the beam spread for the UWB, multiple derivative systems has potentially several interesting applications. The value of the correlation function $\Lambda_{j,mn}^{\text{meas}}$ can be made to increase as the range increases within the near field. This allows the beam launched from a properly designed UWB driven array to maintain its shape as it propagates away from the array. As a result, the efficiency of this beam remains relatively unchanged in the near field. This provides immediate benefits to any application requiring localized fields. For directed energy or radar applications, the derivative transmitter system would also produce an

immediate benefit. It would produce a two-derivative field at the target. Equation (32) indicates that by a proper design of the input field, more intensity would then reach a target than by the corresponding CW system. This behavior is reflected in the enhanced diffraction length given by (33) and the more narrow beamwidth indicated by (41). Depending on how the higher order coherence properties behave under scattering events, one might also be able to reap some further benefit from a derivative receiver system. Recent acoustic LW experiments have shown that those coherence properties are, in fact, maintained in specular reflection events. For a secure communications application, the possibility of encoding information onto the higher order derivatives of the signals exist. Transmitting and receiving such information, for instance, with a three-derivative system, one can design an input field to create a beam which has a substantially narrower profile than the corresponding CW environment. Moreover, since many frequencies are involved, more information could be transmitted with such a system. Similarly, for remote sensing applications, systems with increased depth-of-focus (enhanced diffraction lengths) and beam localization would provide a more accurate probe of a particular medium. Additionally, since a UWB signal contains both high and low wavelengths, the longer wavelengths of the field scattered from an object will contain information about the body resonances of that object and the shorter wavelengths will relay information about its diffraction sites. Because each of its beam characteristics has its own dependence, the advantages of an UWB system will ultimately depend on its specific application.

III. Electrically Short Dipole Transmitter–Receiver System

We will consider an electromagnetic beam generated by an array of electrically short and thin, center-fed, linear dipole antennas and measured in the far-field of each radiator by an electrically short and thin, linear dipole antenna. Because this system is linear, we can first determine the measured signal due to a single pair of radiating elements and then obtain the total response by superposition. This requires a time domain model of the interaction of two center-fed linear dipoles.

A. Elemental Radiator and Receiver

Consider the elemental system shown in Fig. 4. By treating this well-known transmit/receive system in the frequency domain, the corresponding time domain results are then realized by a Fourier transformation. The transmitter system is conveniently divided into two parts: the source and the antenna, which are connected by a transmission line. The voltage source produces the signal $V_{\text{in}}(\omega) = F(\omega)$ at the angular frequency $\omega = kc$. This voltage signal leads to the driving point current $I_1(\omega)$ and the driving point voltage $V_1(\omega)$ at the center of the dipole. The transmitting dipole has length L_1 and the orientation p_1. The characteristic impedance of the source is Z_T, a frequency independent constant over the frequency band

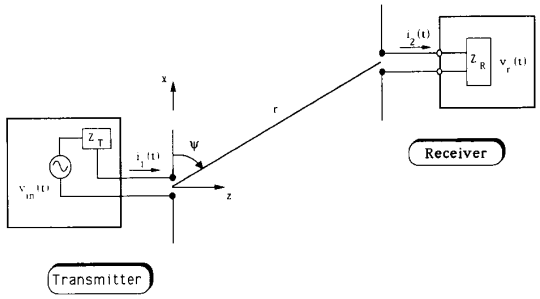

Fig. 4. The basic unit of the transmission/reception system model is a pair of interacting center-fed linear dipole antennas.

of interest. At frequencies well below any antenna resonance, the source impedance Z_T is assumed to be much larger than the antenna impedance and the characteristic impedance of the transmission line. This causes the voltage source to act like a current source. In particular, it causes $I_1(\omega) \approx F(\omega)/Z_T$. The case where the characteristic impedance Z_T is much smaller than the antenna impedance (an ideal voltage source case) [39] also leads to the results presented below; the current source version is notationally simpler and is treated most often in standard texts.

Similarly, the length of the receiving dipole is L_2. The orientation of this dipole is $\hat{p}_2$ and is chosen to maximize the coupling between the two antennas. The induced driving point current and voltage on the receiving antenna are, respectively, $I_2(\omega)$ and $V_2(\omega)$. The output signal $V_r(\omega)$ is measured across the receiver impedance Z_R, a frequency independent constant over the frequency band of interest. This impedance is matched to the transmission line impedance and is much smaller than the antenna impedance so that $V_r(\omega) \approx I_2(\omega)Z_R$.

It is assumed that the transmitting and receiving dipoles are short in comparison to the shortest wavelength of significance contained in the time domain signal driving them, i.e., $kL_m \leq 1$ for $m = 1, 2$. Both of these dipoles are also assumed to be very thin electrically, i.e., if the radius of each dipole is a, then $a \ll L_m$ for $m = 1, 2$. As discussed, for example, by Franceschetti and Papas [26] or Sengupta and Tai [27], the radiated electric field of such electrically short, center-fed linear dipole antennas in the far zone is proportional to the second time derivative of the input voltage signal. Assuming that the transmitting dipole is oriented along the x-axis and is driven with the (voltage) signal $f(t)$, the electric field in the far zone has the time-domain response

$$\vec{e}_t(\vec{r}, t) \approx i\frac{Z_0}{Z_T}\frac{L_1^2}{4}\frac{1}{4\pi r}\partial_{ct}^2 f\left(t - \frac{r}{c}\right)\sin\psi\,\hat{\psi} \quad (45)$$

where the angle ψ is measured from the positive x-axis, i.e., $\psi = \pi/2 - \theta$ and $\hat{\psi} = -\hat{\theta}$, $r = |\vec{r}| = (x^2 + y^2 + z^2)^{1/2}$ is the distance from the center of the transmitting dipole to the observation point (i.e., to the center of the

receiving dipole), and the term Z_0 is the free-space impedance. This result is a very good approximation for the main beam direction (where $\psi \sim \pi/2$); the approximation begins to break down for k-values satisfying $kL_1 > 2$ far away from the main-beam direction. Since the pattern is negligible there and since we are interested in maximal coupling of the dipole antennas, (45) is quite suitable for the following discussions. Note that this result follows quite naturally from a spectrally weighted form of the well-known far-field frequency domain expressions of the field generated by an electrically short, center-fed dipole antenna driven with a sinusoidal current distribution.

The signal measured with an electrically short dipole antenna is the first time derivative of the field incident on it [32], [33]. Consequently, if the receive antenna is assumed to be oriented for maximal coupling, the measured voltage response is

$$v_r(t) \approx i\frac{L_2^2}{4} \sin\psi\, \partial_{ct}\, e_{\text{inc}}(t) \tag{46}$$

which combined with (45) yields the overall response of this elemental, dipole transmitter–receiver system

$$v_r(t) \approx -\frac{Z_0}{Z_T}\frac{L_1^2}{4}\frac{L_2^2}{4}\frac{1}{4\pi r}\,\partial_{ct}^3 f\left(t-\frac{r}{c}\right)\sin^2\psi. \tag{47}$$

This system then has a cumulative three time derivative response. A three time derivative response is also realized with electrically small conical [28], cylindrical [29], and loop antennas [30].

Note, however, that care must be exercised to achieve the same results when dealing with standard frequency domain power arguments. The latter are frequently used to analyze UWB radar systems. Consider the Friis far-field transmission/reception power balance formula

$$P_R(\vec{r},\omega) = \frac{\lambda^2 G_R(\psi,\phi,\omega)G_T(\psi',\phi',\omega)}{(4\pi r)^2}P_T(\omega) \tag{48}$$

which relates the power $P_T(\omega)$ transmitted to the power $P_R(\vec{r},\omega)$ received. One must treat $G_T(\psi,\phi,\omega)$ and $G_R(\psi,\phi,\omega)$ not simply as the gains of the transmitting and the receiving antennas themselves, but of the entire transmitting system and the receiving system, respectively. The transmitted power must then be considered as the power input into the transmitting system: $P_T(\omega) \equiv P_{\text{in}} \sim$ const. Then taking into account not only the intrinsic gain of the antenna, but also the capacitive behavior of the electrically short dipoles in their conversion of the input voltage to the driving current (linear dependence of the impedance on the frequency), the gains $G_T(\psi,\phi,\omega) \sim k^4$ and $G_R(\psi,\phi,\omega) \sim k^4$. One then obtains $P_R(\vec{r},\omega) \sim k^6$ from (48) and, hence, by accounting for the driving signal, the received energy:

$$\mathscr{E}_{\text{rec}} \propto \int_{-\infty}^{\infty} |\partial_{ct}^3 f|^2\, dt \tag{49}$$

which recovers the three-derivative behavior. This argument again points out the need to incorporate the effect of the transmitting and measuring systems on the overall response of the total system, particularly when UWB signals are involved. If only the gains of the antennas themselves had been used, this argument would have led to the incorrect conclusion that the received signal would only be proportional to the first time derivative of the driving signal rather than the third derivative.

B. Transmitting Array and Receiver Model

Consider now an array of N independently addressible, center-fed linear dipoles driven with an arbitrary set of UWB signals. The dipoles in the transmitting array are assumed to be located at the points $\vec{r}_j$ in space in such a manner that the array has a well-defined axis broadside to the array along which the observation point lies. Every dipole in the array is assumed to have the same orientation along the x-axis. The jth element in the array has the radiating area $A_j = (1/2)L_j^2/4$; the total physical area of the array is $A = \sum_{j=1}^{N} A_j$. Since the transmitting dipole is omni-directional, the factor of $(1/2)$ is associated with the radiating area here to account for the energy lost to the half-sphere pointing into the region $z < 0$. The jth element is excited with the driving function $f_j(t)$. The only constraint on the driving functions will be that they be continuous. The associated frequency spectra will be labeled $F_j(\omega)$. Mutual coupling effects between the dipoles are assumed to be small. More detailed models such as those used in [13]–[18] could be constructed which would incorporate those effects for the end-fire case.

The receiver is then assumed to be a single dipole of length L_r whose center is located at the point $\vec{r} = (0, 0, z)$ on the axis of the array and whose orientation is perpendicular to that axis and parallel to that of the transmitting dipoles. The radiating area $A_R = L_r^2/4$ is associated with the receiver. Measurements of the field off-axis are taken in the plane perpendicular to the array axis. This allows for a mapping of the pulse shape as it passes by the observation points.

With the assumed configuration and the result (47), the total measured response is

$$v_{\text{meas}}(\vec{r},t) \simeq \frac{Z_0 A_R}{Z_T}\sum_{n=1}^{N}\frac{A_n}{2\pi R_n}\,\partial_{ct}^3 f_n\left(\vec{r}_n, t - R_n/c\right). \tag{50}$$

Since the electric field in the far zone of each dipole has a particular orientation, it has been assumed here that the resulting angular factors lead to a secondary effect. The accuracy of this assumption increases as the observation point is moved further from the array. If the dipoles are symmetrically distributed about the axis of the array, this result is exact. Thus, the measured power density (W/m^2) is

$$\mathscr{S}_{\text{meas}}(\vec{r},t) = \frac{v_{\text{meas}}^2(t)}{Z_R A_R} \simeq \frac{Z_0^2 A_R}{Z_T^2 Z_R} \cdot\left|\sum_{n=1}^{N}\frac{A_n}{2\pi R_n}\,\partial_{ct}^3 f_n\left(\vec{r}_n, t - R_n/c\right)\right|^2 \tag{51}$$

and the measured field energy (Joules) has the form:

$$\mathscr{E}_{\text{meas}}(\vec{r}) = A_R \int_{-\infty}^{\infty} \mathscr{I}_{\text{meas}}(\vec{r}, t)\, dt \simeq \frac{Z_0^2 A_R^2}{Z_T^2 Z_R} \int_{-\infty}^{\infty} \left| \sum_{n=1}^{N} \frac{A_n}{2\pi R_n} \partial_{ct}^3 f_n(\vec{r}_n, t - R_n/c) \right|^2 dt. \quad (52)$$

The bounds on these beam quantities are obtained immediately from the results given in Section II.

C. Dipole Transmitter–Receiver System Performance Bounds

In our model system the input field is the set of input voltage waveforms $v_{\text{in},j}(t) \equiv f_j(t)$. The measured field is the voltage signal $v_{\text{meas}}(t)$. The input field energy at the nth element is then:

$$\mathscr{E}_n^{\text{in}} = \frac{1}{Z_T} \int_{-\infty}^{\infty} |f_n(t)|^2\, dt. \quad (53)$$

Comparing this expression with (2), the constant $C_{\text{in}}^2 = 1/Z_T$. The total, array-weighted input energy is then given by (3). With (52) and proceeding as in Section II, the bound on the beam energy is found to be

$$\Gamma_{3,\text{enrg}}^{\text{meas}} \le \frac{Z_0^2 A_R^2}{Z_T Z_R c^4} \left(\frac{L_{\text{rad}}}{z} \right)^2 \omega_{\text{meas}}^4. \quad (54)$$

Comparing with (18), one finds the constant term $C_3^2/C_{\text{in}}^2 = Z_0^2 A_R^2/Z_T Z_R c^4$. Similarly, from (31) the bound on the maximum beam intensity is obtained:

$$\frac{(\mathscr{I}_3^{\text{meas}})_{\max}(\vec{r})}{\mathscr{E}_{\text{in}}} \le \frac{Z_0^2 A_R}{Z_T Z_R c^4} \left(\frac{A}{\lambda_{\text{rad}} z} \right)^2 \omega_{\text{meas}}^4 \Upsilon_3^{\text{meas}}. \quad (55)$$

Thus one can achieve the enhancements described in Section II for this type of UWB transmitter–receiver system in comparison to its CW counterparts. In particular, they can be obtained with photoconductive systems such as those discussed in [19]–[25].

In order to make a comparison with the intensity bound presented in [12], for instance, the transmitter-receiver system must be restricted to the one time derivative case. Equation (55) can not be used. The quantity considered in [12] is simply the electric field reaching the far field from a planar, finite-sized radiator driven with a frequency bandlimited signal $F(\omega) = 1$ for $\omega \in [\omega_0 - \omega_\delta, \omega_0 + \omega_\delta]$ and $F(\omega) = 0$ for $\omega \notin [\omega_0 - \omega_\delta, \omega_0 + \omega_\delta]$, whose bandwidth is $\text{BW} = 2\omega_\delta$. The maximum value of the received intensity normalized by the energy dissipated in the radiator is given by [12, eq. (13)] as

$$\frac{\max_t |\vec{E}|^2/Z_0}{\mathscr{E}_{\text{in}}/A} \le \left(\frac{A}{2\pi z} \right)^2 \left[\frac{1}{2\pi} \int_{\text{BW}} \omega^2\, d\omega \right], \quad (56)$$

where explicitly $\int_{\text{BW}} \omega^2\, d\omega = 2\omega_\delta(\omega_0^2 + \omega_\delta^2/3)$. Since $\omega_{\text{rad}}^2 = \int_{\text{BW}} \omega^2\, d\omega / \int_{\text{BW}} d\omega = \omega_0^2 + \omega_\delta^2/3$ and $\Upsilon_1^{\text{meas}} = \omega_\delta/\pi$, one has

$$\frac{1}{2\pi} \int_{\text{BW}} \omega^2\, d\omega = \omega_{\text{rad}}^2 \Upsilon_1^{\text{meas}} \quad (57)$$

so that with the identification $C_{\text{in}}^2 = 1/Z_0$ and $C_1^2 = A_R/A$, one can recover the one-time derivative form of (31) from (56), i.e., (56) becomes

$$\frac{(\mathscr{I}_1^{\text{meas}})_{\max}(\vec{r})}{\mathscr{E}_{\text{in}}} \le \frac{C_1^2}{C_{\text{in}}^2 A_R} \left(\frac{A}{\lambda_{\text{rad}} z} \right)^2 \Upsilon_1^{\text{meas}}. \quad (58)$$

This intensity bound is readily extended to the one time derivative transmitter–receiver dipole antenna systems considered in [13]–[18] and to the driving waveforms obtained by the optimization methods considered there. The energy bound (18) can also be used to recover the bounds on the signal energy measured within a restricted time window derived in those later references.

IV. Numerical Results

The simulation results for the acoustics case reported in [11] can be transferred immediately to the present electromagnetics case. One need only adjust the wave speed and some constant coefficients. Typical results will be presented below to illustrate the performance enhancements possible with a properly designed ultra-wide bandwidth system. In particular, the LW results will be compared to the CW signal whose frequency coincides with the effective frequency of the LW radiated field: $\omega_{\text{CW}} \equiv \omega_{\text{rad}}$. Results associated with CW signals defined by a spectral point criterion such as the 3 dB frequency value of the LW input field will also be reported. These results have been verified experimentally in the acoustics case. A similar electromagnetics experiment will be suggested in the next section. The singular (infinite derivative) cases discussed in Section II will be avoided since they are not physically realizable.

Note that a true CW signal theoretically has an infinite duration and is thus not physically realizable. It has been shown [19] that an array driven with a time windowed CW signal (a CW tone burst) is slightly less efficient than one driven with a pure, infinite duration CW signal because more energy will leak into its sidelobes. The bounds derived in Section III are thus the most stringent possible. The numerical comparisons made below will deal with finite duration CW tone bursts. Since the tone bursts needs about four or five cycles to establish its CW nature, each CW case will deal with several periods.

Given the assumed dipole array, one has only the freedom of choosing the input signals to impact the resulting beam. In the CW input field case the radiated and measured values of the beam energy and intensity will essentially be the same. However, the quality of the near-field beam of a uniformly driven CW array is poor because large constructive and destructive interference regions are formed. The efficiency of the CW beam in its near field will then exhibit the characteristic Fresnel zone peaks and valleys. In contrast, the beam launched from an

LW driven array maintains its shape as it propagates away from the array. The moving interference pattern behavior of the LW beam governs its near-field properties. As a result, the efficiency of this beam remains relatively unchanged in the near field of that array.

Consider the LW solution known as the modified power spectrum (MPS) pulse [3]:

$$u(\vec{r},t) = \mathcal{RE}\frac{1}{z_0 + i(z-ct)}\frac{1}{[(s/\beta)+a]^{\alpha}}e^{-bs/\beta} \quad (59)$$

where $s(\rho,z,t) = \rho^2/[z_0 + i(z-ct)] - i(z+ct)$ and the transverse distance $\rho = \sqrt{x^2+y^2}$. The operator $\mathcal{RE}$ takes the real part of the entire expression to its right. The parameters that will be used here and that have been used for all of the ultrasound experiments in water are $a = 1.0$ m, $\alpha = 1.0$, $b = 6.0 \times 10^2$ m^{-1}, $\beta = 3.0 \times 10^2$, and $z_0 = 4.5 \times 10^{-4}$ m. The speed of light $c = 3.0 \times 10^8$ m/s in air is significantly larger than the speed of sound in water $c = 1.50 \times 10^3$ m/s. This fact modifies the spectral frequencies in the pulse, but not its wavelengths. The MPS solution has the maximum frequency $f_{\max} = c/(2\pi z_0) = c/\lambda_{\min}$ that represents here the $1/e$-folding point of the amplitude of its Fourier spectrum. It also has the transverse waist $w = (\beta z_0/b)^{1/2}$ at $z = t = 0$ and the minimum frequency $f_{\min} = bc/(2\pi\beta)$.

In the following comparisons the broad-bandwidth case will be the LW folded array introduced in [3]. The folded array represents an attempt to include more information about an exact LW solution such as the MPS pulse into the array driving signals. The conformal mapping used for the folded array is simply $\rho \to R_{\max}^2/\rho$, which maps an annulus with its radii greater than the maximum array radius $R_{\max}$ into an annulus with its radii smaller than $R_{\max}$.

Because the calculations are not readily tractable through analysis in this folded array case, numerical simulations will be used to illustrate the major points. The actual driving signals were chosen from a modified version of the folded array scheme proposed in [3] and the MPS pulse (59). Explicitly, a radiating element at (x,y) in the array is driven with the signal:

$$f(x,y,t) = w(t) \times u(\rho, z=0, t), \qquad (\rho = 0)$$

$$f(x,y,t) = w(t) \times \left[u(\rho, z=0, t) + (R_{\max}/\rho)^4 u(R_{\max}^2/\rho, z=0, t-t_d)\right], \qquad (\rho \neq 0) \quad (60)$$

where $R_{\max} = [x_{\max}^2 + y_{\max}^2]^{1/2}$ is the maximum radius of the source locations in the array and the position dependent delay time $t_d = \{[z_d^2 + (R_{\max}^2/\rho)^2]^{1/2} - [z_d^2 + \rho^2]^{1/2}\}/c$, the constant delay distance being $z_d = 3.0 \times 10^{-2}$ m. If the function

$$h(t,\tau) = 0.42 - 0.50 \times \cos[2.0\pi(t/\tau)] + 0.08 \times \cos[4.0\pi(t/\tau)] \quad (61)$$

the extra window function

$$w(t) = \begin{cases} 0, & \text{for } t < -t_1 \\ h(t,t_1), & \text{for } -t_1 < t < -t_2 \\ 1.0, & \text{for } -t_2 \le t \le +t_3 \\ h(t,t_4), & \text{for } +t_3 < t < +t_4 \\ 0, & \text{for } t > +t_4 \end{cases} \quad (62)$$

where the constants $t_1 = 3.0 \times 10^{-11}$ s, $t_2 = 1.5 \times 10^{-11}$ s, $t_3 = 2.5 \times 10^{-12}$ s, and $t_4 = 5.0 \times 10^{-12}$ s. The time window $w(t)$ is included in the driving signals to remove the precursor wings characteristic of the regular MPS driven arrays, hence, to minimize specifically the amount of wasted energy in those wings. The pulses (60) were optimized by varying the associated constants and testing their performance numerically. The desired performance, a more than ten fold enhancement of the measured energy diffraction length, was obtained experimentally with an ultrasound array in water that was driven with these signals [10].

In order to relate the present results to those in [10] and [11], consider a 25-element, 5×5 square array. The elements in the array all have the same lengths $L = 0.5$ mm = 500.0 μm. They are separated by 2.5 mm and are centered in 6.25×10^{-2} cm^2 areas. The total length of the array on a side is thus 1.25 cm and the total area is $A = 1.5625$ cm^2. The small number of elements of radiating elements limits the number of CW configurations; there are too few elements to permit effective shading or focusing.

The LW folded array is driven with six unique signals defined by (60). The effective frequency of the radiated far field is $f_{\text{rad}} = 66.0$ GHz. This value was obtained numerically with the signal processing code SIG [40]. This effective frequency value gives the radiated field energy diffraction length $L_{1,\text{enrg}}^{\text{meas}} = L_{\text{rad}} = 3.44$ cm. Similarly, the effective frequency associated with the measured far field is $f_{\text{meas}} = 287.0$ GHz. This effective frequency value gives the measured field energy diffraction length $L_{3,\text{enrg}}^{\text{meas}} = (f_{\text{meas}}/f_{\text{rad}})^2 \times L_{1,\text{enrg}}^{\text{meas}} = 18.91\ L_{\text{rad}} = 65.05$ cm. In terms of point quantities for the effective frequency, it was found that 50, 63, 87 and 95% of the input energy, respectively, was below 18.4, 27.0, 66.0, and 100.0 GHz. Thus, the $1/e^2$ frequency point coincides with the radiated energy effective frequency. The 3 dB point value for the effective frequency of the radiated field is $f_{3\,\text{dB}} = 18.4$ GHz giving $\omega_{\text{rad}}/\omega_{3\,\text{dB}} = 3.59$. At 100 GHz the term $kL \sim 1.0$ so that the electrically short approximation is valid for all of the elements in this array.

For theoretical comparisons, the array was driven uniformly with a CW tone burst at the frequency $f_{\text{CW}} = 66.0$ GHz. The tone burst is explicitly defined by the signal $f_{\text{CW}}(t) = w(t)\sin\omega_{\text{CW}}t$, where the window function $w(t) = h(|t|,\tau)$, $\tau = 60.6\mu$s. Thus there are approximately six full cycles in the tone burst. The improvement of the measured field energy efficient with the LW drive over the CW drive is then predicted to be an $(f_{\text{meas}}/f_{\text{rad}})^4 = 345$-fold enhancement.

The numerical simulation used here to test these LW pulse-driven array enhancements was a direct time domain implementation of (50). In Fig. 5 the renormalized measured field energy efficiencies $\Gamma^{meas}_{3,enrg}(z)$ for the LW and CW pulse-driven arrays are compared. There are 33 data points on each curve, every third one being labeled by the symbols listed in the legends. The "unscaled" values refer to the numbers resulting directly from (50). The "scaled" values are obtained by multiplying the unscaled values by (1) a factor of two to compensate for the bipolar nature of the CW signals (the actual input energy in the CW case is twice the energy in a half-period, hence, twice its average value) and (2) by the appropriate ratio of the radiated and measured field effective frequencies and the 3 dB point-value for the effective frequency to account for the difference between the energy delivered to the array elements versus the energy launched into the medium which, for the measured energy efficiency, is: $(\omega^2_{rad}\omega^4_{meas}/\omega^6_{3\,dB})/(\omega_{meas}/\omega_{rad})^4 = (\omega_{rad}/\omega_{3\,dB})^6 = 2.13 \times 10^3$.

From Fig. 5 one can see that the unscaled and scaled LW folded array measured field energy efficiencies are much greater than the corresponding CW values. The far-field $1/z^2$ decay rate begins between 50 and 60 cm, roughly 17 L_{rad}, which is in very good agreement with the predicted value of 18.91 L_{rad}. In the far field the LW beam efficiencies show, respectively, a 307.3 and 1.31×10^6-fold improvement over the CW beam. The unscaled value, 307.3, compares quite favorably with the predicted 345-fold improvement. The scaled value, 1.31×10^6, illustrates how large the differences between the LW and the CW cases can be. Either case clearly demonstrates that the LW pulse-driven array outperforms its CW counterpart.

In Fig. 6 the waists of the CW and LW measured field energy profiles are given. These waists are defined as the half-widths at half-maximum (HWHM) of the beam profiles in a plane perpendicular to the line-of-sight direction. The slopes of the CW and LW beam waist curves are, respectively, $\theta^{meas}_{enrg,CW} = 0.16$ and $\theta^{meas}_{enrg,LW} = 0.022$. Thus the CW measured beam energy profile is expanding 7.26 times faster than the LW profile.

The numerical results clearly demonstrate the improvements that are available from LW pulse-driven arrays. The measured LW beams can be made to be more efficient and narrower than their CW counterparts. Similarly, the radiated intensity of the beam generated by the LW pulse-driven array can be designed to be significantly higher than its CW counterpart. These beam enhancements have been confirmed experimentally [10].

Consider again the CW pulse-driven array. The amplitudes of these signals are tapered (amplitude tapering or shading) across the array in practice to achieve a large reduction in sidelobe levels. This is accomplished with an acknowledged loss of beam directivity and a broadening of the main lobe. The main lobe can be made brighter with an increase in the frequency of the driving signal; however, without additional amplitude tapering, higher sidelobe levels will result. Eventually, if one were to raise the frequency of the driving signals to a value where the corresponding wavelength is smaller than the element separation, then the resultant CW beam will contain significant grating lobes. This is a particularly acute problem when the array is sparsely populated with elements. As noted above, the broad-bandwidth LW pulse-driven array can be designed to avoid this problem. This is illustrated in Fig. 7. The theoretical measured-field beam intensity profile for the folded MPS pulse-driven array is compared directly to the measured-field profiles of the beams generated by driving that array with CW tone bursts at 100.0 and 400.0 GHz. These curves were obtained in the plane $z = 30.0$ cm by searching the time history at a given radius and $z = 30.0$ cm for its maximum value and then plotting that value against its ρ value. The intensity profiles are all normalized to unity along the z-axis. There are 101 data points in the profiles; ρ ranges

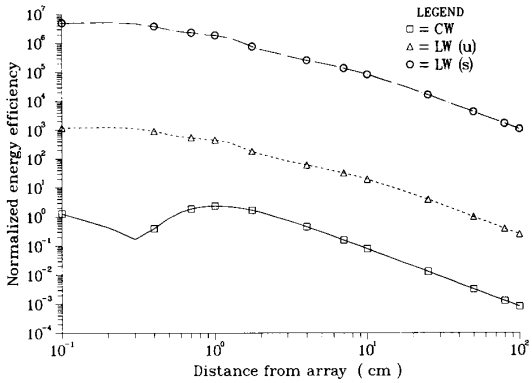

Fig. 5. Comparison of the decay of the measured field energy along the line-of-sight direction of the beams generated by the LW and CW pulse-driven, three derivative model, transmitter–receiver systems. The CW array is driven with the effective radiated frequency of the LW signals: $f_{CW} = f_{rad} = 66.06$ GHz. Both the unscaled (u) values of the LW beam energy efficiency normalized to the CW case, and those values scaled (s) to the corresponding 3 dB frequency CW case: $f_{3\,dB} = 18.4$ GHz, are given.

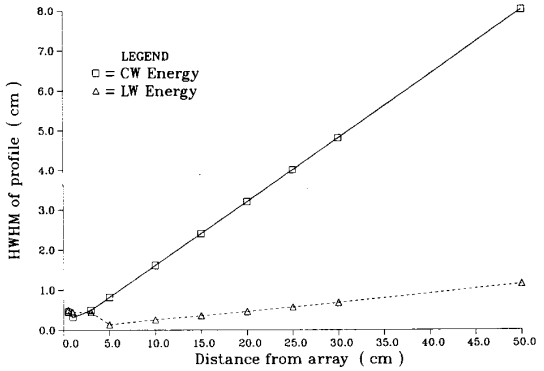

Fig. 6. Comparison of the expansion (half-width at half-maximum) along the line-of-sight direction of the measured field energy profile of the beams generated by the LW and CW pulse-driven, three derivative model, transmitter–receiver systems.

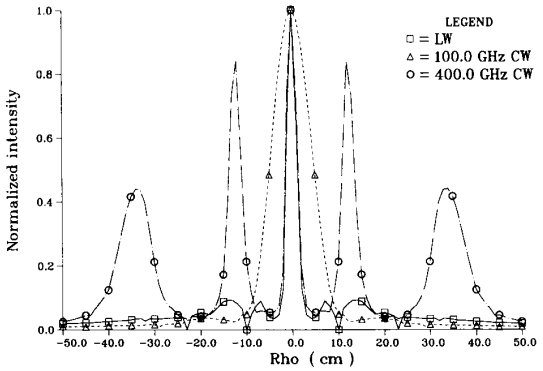

Fig. 7. Comparison of the normalized measured field intensity profiles at $z = 30.0$ cm of the beams generated by the LW and 100.0 and 400.0 GHz CW pulse-driven, three derivative model, transmitter–receiver systems.

from -50.0 to $+50.0$ cm. The wavelength at 100.0 GHz is 3.0 mm, slightly larger than the element spacing of 2.5 mm. On the other hand, at 400.0 GHz the wavelength is 0.75 mm, much smaller than the element spacing. As shown in Fig. 7, the broader beam profile of the 100.0 GHz case is traded for the narrower main lobe and large grating lobes in the 400.0 GHz case. The folded array beam has a main lobe similar to the higher frequency CW case and sidelobe levels similar to the lower frequency CW case. These quantities of the LW beam make it very appealing for a variety of applications.

V. Conclusion

The possibility of generating UWB beams from an electromagnetic array with diffraction lengths or near-field distances much larger than anticipated from conventional CW theory was addressed in this paper. This was accomplished by investigating and understanding the physics and engineering of driving arrays with a spatially distributed set of UWB pulses. Bounds were derived that refine the meaning of a diffraction length and a diffraction-limited beam, particularly for those excitations. It was shown that one can design a multiple time derivative transmitter–receiver system and a set of driving signals specifically for that system which can extend the near field further from its transmitter with a more localized beam than is possible with a comparable CW system. The LW source-free solutions introduced in [3] were then used to illustrate such a set of "designer pulses."

The utilization of an extended frequency set to drive the array introduces beam characteristics which result from different portions of the given frequency set. The bounds presented in Section II were derived in terms of average and point quantities that characterize those frequency subsets. The enhanced localization properties and diffraction lengths of the resulting beams are closely connected with the existence of these additional frequency subsets which do not exist in the CW or narrow-bandwidth cases. They were shown to be particularly important when the transmitter–receiver system involves multiple time derivatives. A pulse-driven transmitter–receiver system model constructed from electrically short dipole antennas was introduced in Section III. The diffraction lengths and bounds for the beam associated with such a three time derivative system were immediately obtained from the results given in Section II. It was then clearly demonstrated in Section IV with numerical results that the LW beams can be designed to outperform their CW counterparts.

Diffraction-free beams with finite energy do not exist, as pointed out in [3] and [41]; and since we are dealing only with linear phenomena, no new frequency content can be introduced into the resulting beams either by the transmitter, the medium, or the receiver than is present in the signals delivered to the transmitting array. The arguments presented here indicate that there are frequency values which effectively characterize the properties of a UWB pulse-driven transmitter–receiver system and that these specific values represent useful choices for comparisons between UWB and CW systems. These arguments also indicate that performance enhancements of the associated beams can be accomplished in the UWB case through frequency shading as well as amplitude shading of the pulse-driven arrays. If the transmitting and receiving arrays behave equally for all driving and received signals, the only control over the beam characteristics one has is through the driving functions. One must properly shape the frequency spectra of the input field to take into account the frequency responses of the transmitting array and the measurement process (receiving array). Beams *can be* generated by UWB pulse-driven transmitter–receiver systems that act as moving interference patterns with extended localization properties. The LW solutions simply provide an immediate access to these enhancements.

The electromagnetics results presented here are straightforward extensions of their experimentally verified acoustic counterparts. Experimental verification of these electromagnetics results is possible. Recent progress in sources of ultra-wide bandwidth electromagnetic energy such as photoconductive/optoelectronic switch technology [19]–[25] provides one with the means of generating 0.1-100 ps wide pulses, which correspond to frequencies of 0.01-10.0 THz. The three derivative dipole-dipole interaction behavior of the transmissioon/reception system modeled here is verified by the experimental work of van Exeter and Grischkowsky [19]. They have been characterizing an optoelectronic terahertz beam system which consists of two broad-bandwidth dipole antenna structures, which are 20 μm in size. The transmitting antenna is driven by a photoconductive switch in its gap region, the switch being excited with a pulsed (70 fs) laser source. The measured time signal and its spectrum are shown in [19, figs. 2 and 3]. The laser excitation pulse is Gaussian in shape; the current $i_{in}(t)$ in the photo-conductive switch obtains a similar but broadened form. The measured voltage signal is two time derivatives of that current pulse.

Since this antenna is electrically small and hence, mainly capacitive with capacitance C, the input voltage $v_{in}(t)$ is related to the driving current as $C\,\partial_t\, v_{in}(t) = i_{in}(t)$. This means the measured voltage signal $v_{meas}(t) \propto \partial_t^3\, v_{in}(t)$. The wavelength at the $1/e$ amplitude roll-off point in that spectrum is approximately 3.0×10^{-2} cm, only an order of magnitude smaller than the case considered here. The MPS pulses presented here are easily adjusted to that frequency regime.

The results presented here also indicate that current systems employing antennas that attempt to reproduce the incident signal waveforms could be improved by introducing (time) derivative detectors, particularly in low signal-to-noise (S/N) environments. This is also confirmed by the experimental work of van Exeter, Fattinger, and Grischkowsky reported in Ref. 20. They significantly improved the measured beam power ($\sim 15\times$ increase) by introducing a time derivative detector in their system, the ultra-fast dipole antenna later used in the system described in [19].

With a properly designed set of optical fiber delay-lines (to deliver laser pulses to each radiating dipole at the correct time) and transmitting dipole antennas (to achieve the requisite variations in the driving signals), a folded MPS array beam could be generated with an optoelectronic THz dipole array. A scaled version of the results presented here could then be tested experimentally. Of particular interest is the cross-talk between radiating elements in the array. This aspect of the array performance is difficult to model analytically or numerically, for even the modest number of elements in the proposed array. Less than 10 elements are dealt with in [15]–[17]; considerable computer resources would be needed to model in the same detail an array with $100^2 = 10{,}000$ elements. In the acoustics case cross-talk was shown not to be an issue because the piezoelectric transducers used were not efficient radiators and the distance between the transducers was large enough, i.e., for pulse width $\tau_{ac} \sim 2$ μs, the associated distance $c_{ac}\tau_{ac} \sim 3.0 \times 10^{-1}$ cm is approximately the distance between the radiating elements in the acoustic array. Thus, most of the energy is radiated away from the array before any significant interaction between its elements can occur. Even though the optoelectronic dipole antennas appear to be much better radiators than the acoustic transducers are, it is anticipated that cross-talk will also be a nonissue in the electromagnetics case. For a pulse width $\tau_{em} \sim 1$ ps, the associated distance $c_{em}\tau_{em} \sim 3.0 \times 10^{-2}$ cm, approximately the distance between the radiating elements in the scaled array. Thus, most of the electromagnetic energy would be radiated away from the array before any significant interaction between the dipole elements could occur. These arguments of course assume a broadside case as was considered above. As shown, for instance, in [15] and [16], the end-fire case would have to be treated more carefully.

Significant physics issues remain in regards to LW pulse-driven arrays and UWB systems in general. These include analyzing the behavior of UWB beams when they are scattered from targets and when they interact with dielectrics and metals such as radar absorbing materials. Important engineering issues also remain, particularly with respect to the physical realization of UWB electromagnetic beams. These include the need for the design and the analysis of hardware (sources, couplers, power splitters, duplexers, receivers, etc.) that will effectively handle UWB signals. Applications-specific investigations into the ramifications of designing enhanced UWB systems, such as a LW pulse-driven transmitter–receiver system, in the areas of remote sensing, communications and directed energy (sonar, radar) systems are currently in progress. The preliminary results are very positive and will be reported elsewhere.

Acknowledgment

The author is deeply indebted to Prof. Donald G. Dudley of the Department of Electrical and Computer Engineering at the University of Arizona; Prof. Ioannis M. Besieris of the Bradley Electrical Engineering Department at Virginia Polytechnic Institute and State University; and Dr. Kendall F. Casey of JAYCOR for their many useful suggestions concerning this work and paper. The author would like to acknowledge Dr. Donald Cooper of Rockwell International and Lawrence Livermore National Laboratory's O-Division for his suggestion that optoelectronic terahertz systems could potentially be used for an experimental realization of the electromagnetic LW beams.

References

[1] J. B. Brittingham, "Focus wave modes in homogeneous Maxwell's equations: Transverse electric mode," *J. Appl. Phys.*, vol. 54, pp. 1179–1189, 1983.

[2] R. W. Ziolkowski, "Exact solutions of the wave equation with complex source locations," *J. Math. Phys.*, vol. 26, pp. 861–863, 1985.

[3] ——, "Localized transmission of electromagnetic energy," *Phys. Rev. A*, vol. 39, pp. 2005–2033, 1989.

[4] A. M. Shaarawi, I. M. Besieris, and R. W. Ziolkowski, "A bidirectional traveling plane wave representation of exact solutions of the scalar wave equation," *J. Math. Phys.*, vol. 30, pp. 1254–1269, 1989.

[5] P. D. Einziger and S. Raz, "Wave solutions under complex space-time shifts," *J. Opt. Soc. Am. A*, vol. 4, pp. 3–10, 1987.

[6] E. Heyman and L. B. Felsen, "Complex-source pulsed-beam fields," *J. Opt. Soc. Am. A*, vol. 6, pp. 806–817, 1989.

[7] P. Hillion, "Spinor focus wave modes," *J. Math. Phys.*, vol. 28, pp. 1743–1748, 1987.

[8] A. M. Shaarawi, I. M. Besieris, and R. W. Ziolkowski, "A novel approach to the synthesis of nondispersive wave packet solutions to the Klein–Gordon and Dirac equations," *J. Math. Phys.*, vol. 31, pp. 2511–2519, 1990.

[9] R. W. Ziolkowski, D. K. Lewis, and B. D. Cook, "Evidence of localized wave transmission," *Phys. Rev. Lett.*, vol. 62, 147–150, 1989.

[10] R. W. Ziolkowski and D. K. Lewis, "Verification of the localized-wave transmission effect," *J. Appl. Phys.*, vol. 68, pp. 6083–6086, 1990.

[11] R. W. Ziolkowski, "Localized wave physics and engineering," *Phys. Rev. A*, vol. 44, pp. 3960–3984, Oct. 1991.

[12] R. E. McIntosh and J. E. Sarna, "Bounds on the optimum performance of planar antennas for pulse radiation," *IEEE Trans. Antennas Propagat.*, vol. AP-30, pp. 381–389, 1982.

[13] D. M. Pozar, R. E. McIntosh, and S. G. Walker, "The optimum feed voltage for a dipole antenna for pulse radiation," *IEEE Trans. Antennas Propagat.*, vol. AP-31, pp. 563–569, 1983.

[14] D. M. Pozar, D. H. Schaubert, and R. E. McIntosh, "The optimum

transient radiation from an arbitrary antenna," *IEEE Trans. Antennas Propagat.*, vol. AP-32, pp. 633–640, 1984.
[15] D. M. Pozar, Y.-W., Kang, D. H. Schaubert, and R. E. McIntosh, "Optimization of the transient radiation from a dipole array," *IEEE Trans. Antennas Propagat.*, vol. AP-33, pp. 69–75, 1985.
[16] Y.-W. Kang and D. M. Pozar, "Optimization of pulse radiation from dipole arrays for maximum energy in a specified time interval," *IEEE Trans. Antennas Propagat.*, vol. AP-34, pp. 1383–1390, 1986.
[17] J. R. Bayard and D. H. Schaubert, "Transient response of a receiving dipole array: Bounds and maximization," *IEEE Trans. Electromagn. Compat.*, vol. 30, pp. 122–129, 1988.
[18] ——, "Target identification using optimization techniques," *IEEE Trans. Antennas Propagat.*, vol. 38, pp. 450–456, 1990.
[19] M. van Exeter and D. R. Grischkowsky, "Characterization of an optoelectronic terahertz beam system," *IEEE Trans. Microwave Theory Tech.*, vol. 38, pp. 1684–1691, 1990.
[20] M. van Exeter, C. Fattinger, and D. R. Grischkowsky, "High-brightness terahertz beams characterized with an ultrafast detector," *Appl. Phys. Lett.*, vol. 55, pp. 337–339, 1989.
[21] Y. Pastol, G. Arjavalingam, J.-M. Halbout, and G. V. Kopcsay, "Coherent broadband microwave spectroscopy using picosecond optoelectronic antennas," *Appl. Phys. Lett.*, vol. 54, pp. 307–309, 1989.
[22] C. R. Lutz and A. P. deFonzo, "Far-field characteristics of optically pulsed millimeter wave antennas," *Appl. Phys. Lett.*, vol. 54, pp. 2186–2188, 1989.
[23] X.-C. Zhang, B. B. Hu, J. T. Darrow, and D. H. Auston, "Generation of femtosecond electromagnetic pulses from semiconductor surfaces," *Appl. Phys. Lett.*, vol. 56, pp. 1011–1013, 1990.
[24] X.-C. Zhang, J. T. Darrow, B. B. Hu, D. H. Auston, M. T. Schmidt, P. Tham, and E. S. Yang, "Optically induced electromagnetic radiation from semiconductor surfaces," *Appl. Phys. Lett.*, vol. 56, pp. 2228–2230, 1990.
[25] N. Froberg, M. Mack, B. B. Hu, X.-C. Zhang, and D. H. Auston, "500 GHz electrically steerable photoconducting antenna array," *Appl. Phys. Lett.*, vol. 58, pp. 446–448, 1991.
[26] G. Franceschetti and C. H. Papas, "Pulsed antennas," *IEEE Trans. Antennas Propagat.*, vol. AP-22, pp. 651–661, 1974.
[27] D. L. Sengupta and C.-T. Tai, "Radiation and reception of transients by linear antennas," in *Transient Electromagnetic Fields*, L. B. Felsen, Ed. New York: Springer-Verlag, 1976, ch. 4, pp. 181–235.
[28] C. W. Harrison, Jr. and C. S. Williams, Jr., "Transients in wide-angle conical antennas," *IEEE Trans. Antennas Propagat.*, vol. AP-13, pp. 236–246, 1965.
[29] H. J. Schmitt, C. W. Harrison, Jr., and C. S. Williams, Jr., "Calculated and experimental response of thin cylindrical antennas to pulse excitation," *IEEE Trans. Antennas Propagat.*, vol. AP-14, pp. 120–127, 1966.
[30] T. S. M. Maclean, *Principles of Antennas: Wire and Aperture*. Cambridge, U.K.: Cambridge University Press, 1986, pp. 111–113.
[31] R. E. Collin and F. J. Zucker, *Antenna Theory, pt. 1*. New York: McGraw-Hill, 1969.
[32] M. Kanda, "Transients in a resistively loaded linear antenna compared with those in a conical antenna and TEM horn," *IEEE Trans. Antennas Propagat.*, vol. AP-28, pp. 132–136, 1980.
[33] M. Kanda, "Time domain sensors for radiated impulsive measurements," *IEEE Trans. Antennas Propagat.*, vol. AP-31, pp. 438–444, 1983.
[34] I. Stakgold, *Green's Functions and Boundary Value Problems*. New York: Wiley, 1979, pp. 270–272.
[35] A. Siegman, *Lasers*. Mill Valley, CA: University Science Books, 1986, p. 672.
[36] J. Hernandez, R. W. Ziolkowski, and S. Parker, "Synthesis of the driving functions of an array for propagating localized wave energy," *J. Acous. Soc. Am.*, vol. 92, pp. 550–562, 1992.
[37] T. T. Wu, "Electromagnetic missiles," *J. Appl. Phys.*, vol. 57, pp. 2370–2373, 1985.
[38] R. Chengli and W. Changhua, "Choice of excitation in electromagnetic missiles," *Electron. Lett.*, vol. 25, pp. 1321–1323, 1989.
[39] D. G. Dudley and K. F. Casey, "A measure of coupling efficiency for antenna perturbations," *IEEE Trans. Electromagn. Compat.*, vol. 33, pp. 1–9, 1991.
[40] D. Lager and S. Azevedo, "SIG, a general-purpose signal processing program," LLNL Rep. UCID-19912, Rev. 1, Livermore, CA, 1985.
[41] T. T. Wu and H. Lehman, "Spreading of electromagnetic pulses," *J. Appl. Phys.*, vol. 58, pp. 2064–2065, 1985.

Richard W. Ziolkowski (M'87–SM'91) received the Sc.B. degree in physics magna cum laude with honors from Brown University, Providence, RI, and the M.S. and Ph.D. degrees in physics from the University of Illinois, at Urbana, in 1975 and 1980, respectively.

He was a member of the Engineering Research Division at the Lawrence Livermore National Laboratory from 1981 to 1990 and served as the leader of the Computational Electronics and Electromagnetics Thrust Area for the Engineering Directorate from 1984 to 1990. He joined the Department of Electrical and Computer Engineering at the University of Arizona, Tucson, as an Associate Professor in 1990. His research interests include the application of new mathematical methods to linear and nonlinear problems dealing with the interaction of acoustic and electromagnetic waves with scattering objects, plasmas, and dielectric materials.

Dr. Ziolkowski is a member of Sigma Xi, Phi Kappa Phi, the American Physical Societies, and Commission B of the International Union of Radio Science (URSI). He served as the Vice Chairman of the 1989 IEEE/APS and URSI Symposium in San Jose and is currently serving as a member of the URSI Commission B Technical Activities Committee.